Reliability of Marine Structures Program

PREDICTION OF EXTREME RESPONSES FROM LIMITED DATA

P. R. de Jong

Supervised By

Steven R. Winterstein

Supported by

Offshore Technology Research Center

Office of Naval Research

Report No. RMS–36

June 1999

Department of CIVIL ENGINEERING
STANFORD UNIVERSITY

PREDICTION OF EXTREME RESPONSES FROM LIMITED DATA

P. R. de Jong

Supervised By

Steven R. Winterstein

Supported by

Offshore Technology Research Center

Office of Naval Research

Report No. RMS–36

June 1999

Final Technical Report
Reliability Assessment of Ship Structures against Fatigue
ONR Grant Number: N00014-96-1-0641
Stanford: 2-ddz-400

The accomplishments of the research project are advancements in the state of knowledge in the reliability assessment of ship structures against fatigue. Fatigue life of ship structural components is believed sensitive to load events exceeding certain thresholds. Ocean waves are known to be the dominant source of fatigue in ship structures. Thus, this fatigue investigation has spanned three technical areas: direct prediction of fatigue damage in non-Gaussian load environments, prediction of probability of exceeding specified load thresholds in non-Gaussian environments, and simulation and prediction of non-linear, non-Gaussian ocean waves. Some of the methods developed are applicable to many different structural types beyond ship structural components. In these cases, the methods have been additionally tested and verified against wind-turbine fatigue data because turbine-blade fatigue data was available to the project.

In the predicting fatigue damage in non-Gaussian load environments, research has concentrated on the fitting of up to three statistical models to observed load data and on application of these models to predict long-term fatigue accumulation from short-term observed data. A broad variety of statistical models have been fit using the method of moments, and the resulting models have been tested against measured data for ship fatigue and for wind-turbine blade fatigue applications.

In the prediction of exceeding specified load thresholds, use of four-moment Hermite models, analytic formulae, first-order reliability method (FORM), statistical bootstrapping methods, and fitting of various statistical models have all been proposed and tested against measured physical data. Numerical algorithms in the form of computer software have been developed as in an effort to more fully understand these phenomena. Example applications have included prediction of extreme statistics of wind-driven ocean waves, and of motions of a spar production platform subject to these waves.

In the prediction of non-linear non-Gaussian ocean waves, a methodology has been developed to simulate second-order random ocean waves to match a target sea spectrum. The inverse has also been developed: identifying the first- and second-order components underlying a specified wave time-history. The results of both the simulation and identification methodologies can be used to predict consistent wave time-histories at other spatial locations. Results of this methodology have been verified against observed wave time-histories both from field data and from model test measurements.

Reports of these methods and results have been documented in numerous papers and reports. The reports generated from research funded by this project are:

1. RMS-19: Steven R. Winterstein, "The FITS Routine: Fitting Distributions to Multiple Databases and Estimating Combined Extremes" June 1996
2. RMS-22: Alok K. Jha and Steven R. Winterstein, "Wavemaker 2.0: Simulation and Identification of Second-Order Random Waves" June 1996
3. RMS-24: Alok K. Jha, "Nonlinear Random Ocean Waves: Prediction and Comparison with Data" June 1997
4. RMS-25: Alok K. Jha, "Spar Floating Platform: Numerical Analysis and Comparison with Data" June 1997
5. RMS-26: Alok K. Jha, "Non-Linear Ship Loads and Fatigue Reliability" June 1997
6. RMS-27: Alok K. Jha, Steven R. Winterstein, "Cycles 2.0: Fatigue Reliability Models and Results form Wave and Wind Applications" June 1997
7. RMS-33: Bert Sweetman, Alok K. Jha, Steven R. Winterstein, "Second-Order Random Ocean Waves: Prediction of Temporal and Spatial Variation. The Routine WAVEMAKER" June 1998
8. RMS-34: Ron de Jong and Steven R. Winterstein, "Probabilistic Models of Dynamic Response abd Bootstrap-Based Estimates of Extremes: the Routine MAXFITS" June 1998
9. RMS-36: P. Ron de Jong, "Prediction of Extreme Responses form Limited Data" June 1999
10. RMS-37: Bert Sweetman, Steven R. Winterstein, "Second-Order Random Ocean Waves: Prediction of Temporal and Spatial Variation from Fixed and Moving References" May 1999
11. RMS-39: LeRoy M. Fitzwater and Steven R. Winterstein, "Estimation of Extremes from Limited Time-Histories: The Routine MAXFITS with Wind Turbine Examples" May 2000

ABSTRACT

The main objective of this thesis is to study procedures to estimate statistics of extreme responses to random excitation. Various methods are applied to predict the extreme statistics of the horizontal offset of a spar buoy, consisting of 3 dominant frequency bands; resonant surge, resonant pitch, and wave frequency response. In order to study the effect of limited data, both 1 hour of model test data and 36 hours of computer simulated data were analyzed. Gumbel, standard Weibull, quadratic Weibull, and Hermite models were fitted using the method of moments. The local peaks of the components of the response appeared to be well described by the Rayleigh model (of which the Weibull is a generalization) when fitted to the simulated data. The distribution of the total response, being a mixture of 3 Rayleigh distributed variables, was better described by the Hermite (local peaks) and Gumbel distributions (global peaks). For the observed 1 hour of data, the distributions of the components seemed considerably more narrow and "pinched". We show this to be largely due to the effect of limited data, which biases the higher moments in particular. However, it is not unlikely that limitations of the computational model account partly for this discrepancy. Estimates of the uncertainty in our predictions were made using non-parametric bootstrapping, which were compared to results from simulation. The results suggest that computer simulations provide good results, while non-parametric bootstrapping appears to be less suitable to estimate statistics of extremes. In addition, it appears that for all models the uncertainty in the predictions of the mean max can be reduced by dividing the limited data into short-duration segments, from which many estimates of the mean max can be made by extrapolating a fitted model.

ACKNOWLEDGEMENTS

This report documents work carried out during a two-year period in the Reliability of Marine Structures program at Stanford, and is part of the requirements for an Engineer degree. During these two years I have been exposed to a variety of very interesting topics, which I hope to be working with in the future. I want to thank my advisor Dr. Steve Winterstein for his guidance and making my stay at Stanford possible. I am also very grateful to Sverre Haver, who introduced me to the RMS program, and supported and guided me throughout my research. Besides my mentors, I also want to thank my fellow students Alok Jha, Paolo Bazzurro, Nilesh Shome, Jorge Carballo, and Tina Kashef for their help and advice. I want to express my gratitude in particular to Bert Sweetman and Knut Engebretsen, who have been extremely helpful during my research, by sharing their wealth of experience and participating in the various discussions that ultimately lead to this report. Finally I would like to acknowledge funding by Offshore Technology Research center (OTRC).

CONTENTS

INTRODUCTION

Objective

The main objective of this thesis is to study procedures to estimate statistics of extreme responses to random, excitation. The specific application here is to the response of floating structures, though the methods surveyed here have more general applicability. With the exploration of oil and gas in very deep water, such as the Gulf of Mexico, West Africa, and the North Sea, floating structures have become a very important concept for operators, replacing jacket and tower structures. In deep water, jacket and tower structures are at a disadvantage as they become too flexible. Their natural frequencies decrease towards values where there is a significant amount of wave energy, causing dynamic excitation. Floating structures generally have their natural frequencies of oscillation well away from the primary wave frequencies. Although they can still be excited dynamically, they are considerably more cost effective in deeper water.

While wave loads on a jacket or tower structure can be estimated in a fairly straightforward manner with Morison's empirical formula, the loads on floaters generally require more complicated diffraction models. An important complication is that the *dynamic* response of floaters is governed by two random variables, the wave height and the wave period, while in the case of a regular jacket or tower structure only the wave height dominates the *quasi-static* response. The use of more complicated (non-linear) response models complicates the statistical analysis of the response. Various methods, which can be used in the design process will be discussed and applied for a spar buoy in

this report. The accurate prediction of extreme behavior is critical in the design process. The shift to floating structures has created a need for appropriate statistical models. This work is intended to provide some insight and explore some possibilities to address this need.

Background

Limit States

During the design of a structure one has to consider all possible ways the structure can fail, and assure that the probability of failure is sufficiently small. Failure implies that the structure cannot satisfy its functional requirements anymore, which need not be equivalent to collapse. These functional requirements are generally modeled as limit states $M_i(x_1,x_2,\ldots,x_n)$, which can be functions of many random variables. The probability that a certain limit state is exceeded ($M_i < 0$) determines how reliable or safe the structure is with regard to that limit state. The combination of all limit states determines the total probability of failure. Generally a limit state is expressed as $M = R - L$, where R represents the resistance, and L represents the load. More generally, R and L should be considered general "capacity" and "demand" variables respectively. These may be expressed in terms of loads, load effects, or resulting response quantities. Many reliability studies now consider displacement (or ductility) demands, as we will do here. For offshore structures subject to wave loads, the analysis generally comprises of two time-scales, which are typically referred to as "long term" and "short term". The motivation for this divide is that the wave environment, and hence the structural response, is generally a slowly evolving non-stationary random process. Generally this situation is

modeled by assuming the random wave process to be stationary for short-term periods or sea states, and calculating the statistics for a sea state conditional on the long-term environmental parameters, by which it is defined. Both time scales are discussed in the following paragraph.

The Extreme Response

The limit state we are concerned with here, is failure caused by extreme overload due to ocean waves. The particular case we will analyze in chapters 3 and 4 is the extreme horizontal offset of a spar buoy (where, as noted above, the offset is the load L). If the spar exceeds a certain limiting offset (i.e. the resistance R), failure occurs. In many cases the variability in the resistance is negligible compared to the variability in the load, and the problem reduces to the load exceeding a certain deterministic value. The random variables that determine the statistics of the waves (and the response) are the significant wave height Hs, the spectral peak period Tp, and the extreme response X_{max} given these two parameters that define the stationary random process. The quantity Hs determines the area $\sigma_\eta^2 = (Hs/4)^2$, under the wave power spectrum, while Tp corresponds to the frequency with maximum power. The so called "short term" problem is to estimate the statistics of X_{max} given Hs and Tp, while the "long term" problem then includes randomness in Hs and Tp across various sea states. We focus here on the "short term" problem only, assuming Hs and Tp are fixed (coinciding, for example, with available steady state model test conditions). The long term problem can be handled by conventional methods; e.g. Form (Madsen, 1986) or simulation (Melchers, 1987).

The extreme response, X_{max}, will be a random variable, which can be modeled, by considering the response process x(t) over different time scales. The various time scales, and appropriate distribution models for the standard Gaussian case are discussed below. We begin here at the finest time scale, and proceed to increasingly global time scales.

Model of the Entire Process, X(t).

At the finest time scale, we may seek to model the cumulative distribution function (CDF) $F_X(x)$ of the random process x(t) selected at arbitrary time t:

$$F_X(x) = P[X(t) \leq x] \tag{1.1}$$

In the most common case X(t) is assumed Gaussian, in which case $F_X(x)$ can be evaluated numerically in terms of only the mean μ_x and the standard deviation σ_x of the process X(t):

$$F_X(x) = \Phi\left(\frac{x - \mu_x}{\sigma_x}\right) \tag{1.2}$$

In which $\Phi(u)$ is the standard normal distribution function.

Model of Local Peaks, Y.

We may instead choose to ignore all points of the time history except its local peaks, typically defined as the largest peak per upcrossing of the mean level. For a narrow-band normal process, this results in a Rayleigh distribution for Y, which again depends on the mean μ_x and the standard deviation σ_x of the process X(t):

$$F_Y(y) = 1 - \exp\left[-\frac{(y-\mu_x)^2}{2\sigma_x^2}\right] \qquad 1.3$$

For $y \geq 0$ only.

Model of Global Peaks, Z.

Finally we may instead choose the maximum value Z over a still coarser time scale, comprising multiple peaks (e.g., 10-minute maxima, 1-hour maxima). As when proceeding from the process to the local peaks, this step has the advantage of focussing more on the upper tail of interest, and the corresponding disadvantage of using less detailed information about the time history.

Generally the distribution function of Z is commonly estimated from that of Y as follows:

$$F_Z(z) = [F_Y(y)]^N \qquad 1.4$$

In which N here is the number of local peaks (Y values) within the duration over which Z extends (again 10 minutes, 1 hour, etc.). eq 1.4 assumes both that the number of peaks, N, is deterministic and that their levels are mutually independent. Neither assumption is

strictly correct, but corrections commonly become less significant as we consider extremes in the upper tails of the response probability distribution. In the Gaussian case, combining eqs. 1.3 and 1.4 yields the results

$$F_Z(z) = \left[1 - \exp\left(-\frac{(x-\mu_x)^2}{2\sigma_x^2}\right)\right]^N \approx \exp\left(-Ne^{\frac{(x-\mu_x)^2}{2\sigma_x^2}}\right) \qquad 1.5$$

This finally gives us the distribution of the extreme response based on the mean and standard deviation of the process itself and the number of local peaks. Although this result is widely used, the response of a floating offshore structure is generally not Gaussian due to non-linearities in the response that cause non-Gaussian behavior even if the wave process is Gaussian, which it is only by approximation. The various models that are available for X, Y and Z in the non-Gaussian case are discussed in chapter 2. Given arbitrary distributions $F_Y(y)$ or $F_Z(z)$ the global extreme distribution can also be estimated from the distribution of shorter-period global extremes similar to eq. 1.4.

$$F_{X_{max}}(x) = \begin{Bmatrix} [F_Y(x)]^{N_Y} \\ [F_Z(x)]^{N_Z} \end{Bmatrix} \qquad 1.6$$

If F_Y has been fit we use the top expression in equation 1.6, in which N_Y is the number of local peaks expected in time T. If F_Z has been fit, we use the bottom expression in

equation 1.6, in which N_Z is the number of global peaks (e.g. number of 10-minute or 1-hour segments) in time T.

Uncertainty Estimates through Bootstrapping

Finally, bootstrapping methods (e.g., Efron and Tibshirani, 1993) are used here to estimate the statistical uncertainty associated with any/all of our estimated statistics of X_{max}. The method is conceptually straightforward, generating multiple "equally likely" data sets by simulating, with replacement, from the original data set. Thus some of the data values will be repeated multiple times, while others will be omitted, in any single bootstrap sample (which is of the same size as the original data set). The same estimation procedure performed for the original data set is repeated for each of the bootstrapped samples, and the net statistics on the results are collected and reported.

The bootstrap method is "non-parametric" by definition, in that it operates with no additional information beside the actual data values. Alternative approaches might fit a parametric model, either statistical or

physical, to generate additional "equally likely" samples from which to infer sampling variability levels. Such approaches may confer advantages in some cases but are generally problem-specific; the prime virtue of the bootstrap method lies in its generality. We will consider both bootstrapping and parametric, simulation-based approaches here.

Problem Description

Model Tests

For floating offshore structures model tests are often performed in order to verify and calibrate a computational model that can reproduce the observed times trace of the response from the observed wave history. In addition the results can be used to directly estimate the extremal statistics, and the distribution of the global peak of the response for a certain sea state (i.e. for random realizations from a specific wave spectrum characterized by Hs and Tp). An important question that arises for model tests is how accurate the results are, or more precisely how much data must be simulated to obtain the required accuracy.

Statistics of the Extreme Response

As mentioned earlier, the highest response X_{max} in a certain period of time will be a random variable with a certain distribution. We may be concerned with estimating various statistics of this distribution; e.g. the mean hourly max $\mu(X_{max},)$ its standard deviation $\sigma(X_{max},)$ upper fractiles of $X_{max,}$ etc. Once such an estimate is made, a measure of the variability of this estimate, e.g. its standard deviation, would be a second important number to report. If , for example, we have 10 hours of data for a certain phenomenon and are interested in estimating the mean hourly maximum, $\mu(X_{max},)$, we would have 10 "observed" hourly extremes $X_1 \ldots X_{10}$, from which we can determine the sample mean, $\overline{X} = \frac{1}{N}\Sigma X_i$, and the sample standard deviation, $S_X = \sqrt{\frac{1}{N-1}\Sigma\left(X_i - \overline{X}\right)^2}$. The sample

mean would be our best estimate of the 1-hour mean max, $\mu(X_{max,})$. The standard deviation of the mean, which is equal to the standard deviation, s_X, divided by the square root of the number of observations, would measure the accuracy of our estimate.

The first observation is that we use very little of the available data, i.e. only one value per hour. By using very few numbers to estimate the mean or any other statistic, we have a relatively large amount of statistical uncertainty. The question now arises whether it is possible to use more of the available data by fitting a model of e.g. the local peaks, and deriving the distribution of the relevant global peaks, in order to reduce statistical uncertainty of the hourly extreme in this case. The price we pay is that the more data we use, the less relevant the included data points will be to the extreme value we are trying to estimate, increasing model uncertainty.

The Hybrid Method

The hybrid model addresses the problem of data usage by fitting a parametric distribution of the extreme response to each hour in the previous example. As discussed earlier, this approach allows any amount of data between the number of parameters and the entire data set to be included in the estimate, by modeling the process, the local peaks, or the global peaks. From the fitted distribution of Y or Z, the distribution of the extreme response and its mean for that specific hour can be determined. The hope is now that the variability in these 10 estimated means is less than the variability of the 10 observed extreme values, while they are estimates of the same value. The expectation is that there

is an optimal combination between the amount of data used to fit the model and the relevance of the data to the prediction.

Torhaug (1995) applied the hybrid method to determine the extreme response of jack-up structures, specifically modeling either all peaks, Y, or the entire process, X. In this case, he found that the variability could be decreased by a factor of 2.5, which would reduce the amount of required data to achieve the same accuracy with a factor of 6.

Scope and Organization

Chapter 2 discusses methods to fit the data, and probability distributions for the process, the local peaks, and the global peaks. The models that are discussed were implemented in a computer routine "MAXFITS" (De Jong and Winterstein, 1998). The code is based on a distribution library that is also used for the "FITS" routine (Kashef and Winterstein, 1998). The program was used to analyze OTRC spar buoy data to address the problem described in this chapter, and to explain and demonstrate the routine for general use.

Chapter 3 describes the analysis of the spar buoy data in detail. It discusses the distributions of the process, the local peaks, and the global peaks respectively. Estimates of the uncertainty are made, and the various methods are compared using 1 hour of measured data. Chapter 4 compares the results of chapter 3 to results based on a much larger amount of simulated data in order to reduce statistical uncertainty. The chapter concludes with recommendations for "optimal" data use. The final chapter summarizes the findings of this work, and makes recommendations for future research. It is important

to note that this work is limited to the statistical analysis of stationary relatively short periods or sea states. The results are intended to be used in long-term analyses, for which various routines have been developed such as "HTCNTR", "IFORM", and "SURFIT", which is discussed by Engebretsen, 1998.

SOLUTION METHODS AND APPROACHES

Fitting distribution parameters

All probability distributions used here require a limited number of parameters to be determined in way that allows us to describe the data 'best'. What is best is a somewhat subjective issue, although there are several "goodness of fit" measures available (e.g. Benjamin and Cornell, 1971). The following fitting methods can be used:

- Least squares method
- Maximum likelihood estimate
- Method of moments

The least squares fit, which returns distribution parameters that minimize the sum of the squares of the differences between the model and the data, is commonly used. One can imagine that a small change in one of the parameters will hardly affect predictions in e.g. the body of the distribution, but might have a very significant effect on the tail of the distribution. Turning this logic around, different data points are not equally "weighted" in the fit. Their "weight" depends on the type of distribution and is completely arbitrary. This method is not preferred for this reason. An alternative to the least squares fit is the maximum likelihood estimate. This method maximizes a likelihood function, which expresses the likelihood of observing the data set given the set of parameters sought. An analytical solution to this maximization problem is not always available, in which case

numerical methods must be used. The method used here is the method of moments. The parameters are related to the statistical moments, which represent all data in a consistent manner. The analytical expressions for these relations will be worked out further on.

The moments are defined as:

$$\mu_i(x) = \int_{-\infty}^{\infty} x^i f(x) dx \qquad \textit{for } i = 1,2,.. \quad \text{in the continuous case} \qquad 2.1a$$

$$\mu_i(x) = \sum_{All\_x} x^i p(x) \qquad \textit{for } i = 1,2,.. \quad \text{in the discrete case} \qquad 2.1b$$

Where μ_i is the i^{th} moment and $f(x)$ is the probability density function. Usually only the first four central moments are used, from which the true mean (μ), standard deviation (σ), skewness (α_3), and kurtosis (α_4) can be estimated as follows:

$$m_x = \frac{1}{n}\sum_{i=1}^{n} x_i \qquad 2.2$$

$$s_x^2 = \frac{1}{n}\sum_{i=1}^{n} (x_i - m_x)^2 \qquad 2.3$$

$$a_3 = \frac{1}{n}\sum_{i=1}^{n}\left(\frac{x_i - m_x}{s_x}\right)^3 \qquad 2.4$$

$$a_4 = \frac{1}{n}\sum_{i=1}^{n}\left(\frac{x_i - m_x}{s_x}\right)^4 \qquad 2.5$$

where:

m_x	: sample mean of x	s_x	: sample standard deviation of x
a_3	: sample skewness of x	a_4	: sample kurtosis of x
n	: sample size		(sometimes3 is subtracted, as this is α_4 of a normal distribution)

These expressions are the most commonly used, but some may be biased in certain cases. For independently sampled data, the following corrections can be shown to produce unbiased estimates of the quantities σ_x^2, $\alpha_3\sigma_x^3$, and $\alpha_4\sigma_x^4$ (the response cumulants) (Fisher, 1928).

$$s_x^2 = \frac{n}{n-1}\sum_{i=1}^{n}\frac{(x_i - m_x)^2}{n} \qquad 2.6$$

$$s_x^3 a_3 = \frac{n^2}{(n-1)(n-2)}\sum_{i=1}^{n}\frac{(x_i - m_x)^3}{n} \qquad 2.7$$

$$s_x^4(a_4 - 3) = \frac{n^2}{(n-1)(n-2)(n-3)}\left[(n+1)\sum_{i=1}^{n}\frac{(x_i - m_x)^4}{n} - 3(n-1)\left[\sum_{i=1}^{n}\frac{(x_i - m_x)^2}{n}\right]^2\right] \qquad 2.8$$

Eqs. 2.7-2.8 may still produce bias in their estimates of the unitless quantities α_3 and α_4. No general results (independent of distribution type) are available for α_3 and α_4 directly.

Distributions

The choice of what distribution model to use in what situation is very much a property of the data. For Gaussian data the models discussed in chapter 1 suffice. In the non-Gaussian case we need to employ different, more general models. Various alternative distribution models for the process, the local peaks, and the global peaks are discussed in the following paragraphs.

The Process, X

A Gaussian process will plot as a straight line on normal probability scale. Non-Gaussian data will tend to show curvature on this scale. One way to add curvature to the model, is to distort a standard normal distribution such that it plots as a polynomial on normal probability scale. It has been shown by Winterstein, 1988) that a cubic transformation of the standard normal distribution can often capture non-Gaussian aspects due to various non-linear mechanisms. In this form it is generally referred to as the Hermite distribution, which can match the first four moments of the data. Another popular transformation of a normal process is to exponentiate it, leading to a "lognormal" process (i.e. one whose logarithm is normal). This process can match only two moments, however, and its upper tail generally decays too slowly for accurate extreme estimation.

Hermite

The Hermite distribution is a cubic transformation of a standard normal distribution:

$$f_U(u) = \frac{1}{\sqrt{2\pi}} \exp\left(-\tfrac{1}{2}u^2\right) \qquad 2.9$$

where:

$$x = g(u) = m_x + \kappa\sigma_x\left[u + c_3\left(u^2 - 1\right) + c_4\left(u^3 - 3u\right)\right] \quad \text{for } \alpha_4 > 3 \qquad 2.10a$$

$$u = g^*\left(x^*\right) = x^* - c_3\left(x^* - 1\right) - c_4\left(x^{*3} - 3x^*\right) \quad x^* = \frac{x - m_x}{\kappa\sigma_x} \quad \text{for } \alpha_4 < 3 \qquad 2.10b$$

Approximate analytical expressions are available to relate c_3, c_4 and κ to the skewness and kurtosis of the data (Winterstein and Lange, 1995). Alternatively an iteration scheme can be used to find κ, c_3, and c_4.

Local Peaks, Y

In the case of a standard narrow-band normal process u(t), a randomly selected peak v(t) will have a Rayleigh distribution:

$$F_V(v) = 1 - \exp\left(-\tfrac{1}{2}v^2\right) \qquad 2.11$$

The Hermite model then assumes the functional transformation g or g^*, which relates u to x for each time point. It therefore leads to the same transform at the time of peak values:

$$\begin{aligned} y &= g(v) \qquad \alpha_4 > 3 \\ v &= g^*(y) \qquad \alpha_4 \leq 3 \end{aligned} \tag{2.10}$$

Here y describes a peak of the non-Gaussian process, g and g^* are givem in Eq. 10, and v is the Rayleigh distributed peak described by Eq. 2.11.The Hermite model is now used to describe the local peaks, although it has been fitted to the process.

If we desire to model the peaks directly and circumvent the distribution of the process (using less data), the Weibull distribution is the most commonly used. Originally, the Weibull distribution was derived as a type III distribution of global minimum values. It is based on the assumption of peaks occurring with a limited tail of interest. Instead it is often used as a distribution of individual peaks. The Rayleigh distribution and the exponential distribution are special cases of the Weibull.

Weibull

The Weibull distribution is commonly used to model the local peaks of a process.

$$F_Y(y) = 1 - \exp\left[-\left(\frac{y - y_0}{\beta}\right)^{\alpha}\right] \tag{2.12}$$

If α and β are known, the mean and variance are given by:

$$\mu_y = \beta\left(\frac{1}{\alpha}\right)! \qquad 2.13 \qquad \text{and} \qquad \sigma_y^2 = \beta^2\left[\left(\frac{2}{\alpha}\right)! - \left(\frac{1}{\alpha}\right)!^2\right] \qquad 2.14$$

These expressions can be derived by transforming a standard exponential variable to a Weibull variable, and modifying the standard expressions for the moments of a standard exponential distribution accordingly. If instead we estimate μ_y and σ_y^2 directly from data, values of α and β have to be determined from Eqs. 2.13-2.14 by iteration.

The Weibull distribution in its form above will plot as a straight line on Weibull-scale. If the data show curvature, the Weibull distribution can be distorted in a way similar to that done for the normal distribution, leading to quadratic and cubic Weibull distributions. The quadratic model allows the skewness of the peaks to be fitted in addition to the mean and the standard deviation. The cubic model also allows the kurtosis of the peaks to be fitted. As the distribution of peaks is one-sided the quadratic Weibull may often suffice. By trying to fit both the skewness and the kurtosis the result can become unstable when extrapolating in the upper tail. This "overfitting" of the distribution of peaks is discussed in more detail by Kashef and Winterstein (1998).

Often not all the peaks are used to fit the Weibull distribution. Instead, only the peaks above a certain threshold are fitted. The threshold, which may often for example reflect the mean of the process, is represented by the term y_0 in expression 2.12. Alternatively

instead of adding a quadratic expansion, this third parameter can be fitted to the skewness, also causing curvature on Weibull-scale. This however is somewhat indirect as the lower threshold of the distribution is manipulated to better match the upper tail of the distribution to the data. The quadratic expansion on the other hand manipulates the upper tail, and is therefore preferred here.

Quadratic Weibull:

In this model, one relates peaks y of a process, possibly above some user-defined lower limit, y_0, to a standard Weibull variable w by:

$$y - y_0 = \kappa\left(w + \varepsilon w^2\right) \qquad \text{for} \qquad \alpha_{3,y} < \alpha_{3,w} \qquad 2.15$$

$$w = \frac{y - y_0}{\kappa} + \varepsilon\left(\frac{y - y_0}{\kappa}\right)^2 \qquad \text{for} \qquad \alpha_{3,y} > \alpha_{3,w} \qquad 2.16$$

Here w has the standard Weibull distribution:

$$F_Y(w) = 1 - \exp\left[-\left(\frac{w}{\beta}\right)^{\alpha}\right] \qquad 2.12$$

The skewness of the model is matched to the data by changing ε in an iterative process, which does not affect α and β. These follow from the previous expressions (2.13 and 2.14).

Global Peaks

There are three general types of distributions for global extremes; Type I, type II, and type III distributions. Their differences lie in the assumptions made concerning the underlying distribution of peaks. For type I distributions we assume that the upper tail of the underlying distribution of Y falls off exponentially, which is e.g. the case for the Weibull and the Rayleigh distribution. The type I distribution is commonly called the Gumbel model, which is described below.

Gumbel

The Gumbel distribution models the global extremes, Z, and has the following expression:

$$F_Z(z) = \exp[-e^{-\alpha(z-z_{mode})}] \qquad 2.18$$

where γ and z_{mode} are determined from the moments of the global extremes:

$$\alpha = \frac{\pi}{s_z\sqrt{6}} = \frac{1.282}{s_z} \qquad 2.19 \qquad \text{and} \qquad z_{mode} = m_z - \frac{\gamma}{\alpha} = m_z - \frac{0.577}{\alpha} \qquad 2.20$$

where γ is Euler's constant

A Gumbel distribution plots as a straight line on Gumbel probability scale. If the data shows curvature a polynomial expansion can be added similar to the Hermite of the

quadratic Weibull distributions. This is discussed in detail by Winterstein and Haver (1991).

Type II and Type III distributions

A type II distribution assumes a limited tail on the left at zero, but an unlimited tail on the right of the underlying distribution of individual peaks. The general form of the distribution of individual peaks is:

$$F_Y(y) = 1 - \beta\left(\frac{1}{y}\right)^k \qquad \text{for } y \geq 0 \qquad 2.21$$

The distribution of the global peaks, Z, is the distribution of Y raised to the power of the number of individual peaks, assuming independence. This gives after some approximations:

$$F_Z(z) = e^{-\left(\frac{u}{z}\right)^k} \qquad \text{for } z \geq 0 \qquad 2.22$$

Type II distributions are related to type I distributions in a similar fashion as the lognormal distribution is related to the normal distribution, i.e. $Z_I = \ln Z_{II}$, where Z_I has a type I, and Z_{II} has a type II distribution. Contrary to Type I distributions, Type II and III distributions are ill-suited to our moment-fits, due to potential moment divergence (Type II) or to the difficulty in predicting truncated distributions (Type III) from moment information.

SPAR BUOY RESULTS BASED ON 1HR OF MODEL TEST DATA

Introduction

Recently the first two production spars have been built. The Neptune, operated by Oryx was installed in 1996, while Chevron installed its Genesis platform in 1997. A third spar is under construction for the Diana field, which will be operated by Exxon. Presently production spars are considered by many operators as a very competitive concept for water depths ranging from roughly 2000 to 6000 ft, offering important advantages over tension leg platforms (TLPs) and semi-submersibles.

In principle a spar buoy is a very large vertical cylinder, providing buoyancy to support production facilities, and optionally to store oil. The structure is kept in place by mooring lines, which can be either catenary or taut. The latter concept may require the use of polyester lines and is an upcoming solution for deep water. It provides restoring forces through the elastic properties of the material, in addition to the restoring forces resulting from the geometry and weight of the lines, which give a catenary mooring system its stiffness. The horizontal stiffness of the spar system is determined by the mooring system, while the vertical stiffness is determined by hydrostatic properties, which are determined by the geometry of the hull. The moorings and the structure are designed such that natural periods are well above the dominant wave periods. Natural periods for the different modes of a production spar are generally in the order of minutes, while wave periods are in the order of seconds. Nevertheless dynamic excitation can occur, which is discussed in the following paragraphs. Damping is caused by loss of energy through

turbulence and friction, and is generally difficult to quantify. We include here the effects of viscous damping, radiation damping and wave drift damping. The mass of the system is the mass of the spar buoy plus the mass of the water entrapped in the center well, and the added mass of the water around the structure. The reader can refer to e.g. Glanville et al (1991), for more general information about the spar buoy concept.

The Model Test

The data that is analyzed here is the result of a joint industry project, carried out by the Offshore Technology Research Center at Texas A&M. Model tests were run for a spar buoy with a catenary mooring system. The characteristics of the structure are summarized in table 3.1. The prototype scale, on which all values are reported, is 1:55.
The results have been used to study the accuracy of various computational models that can predict structural response accurately (e.g. Ran et al., 1996, Weggel and Roesset, 1996, or Mekha and Roesset, 1995). Issues that were of particular interest were the damping and viscous forces. Different conditions were simulated, of which one realization of a100 year extreme unidirectional Gulf of Mexico (GOM) storm without current was selected for the analysis here. The characteristics of this sea state are listed in table 3.2. The following data has been used from these tests:

- The undisturbed (far field) wave elevation, measured at an along-wave point, during the actual model test.
- The disturbed wave elevation near the structure
- Horizontal offset of the spar at 54.8 m above MWL, along the vertical cylinder axis

- Pitch rotation
- Heave motion

The horizontal offset is the combined effect from surge and pitch motions. In general besides the motions mentioned above, also lateral horizontal motion or sway, caused by vortex induced vibrations (VIV) can be significant. In practice, these motions are reduced by helical strakes on the hull, which can be seen in figure 3.2. Sway will not be discussed here. For the analysis only the horizontal offset data at 54.8 m MWL was used.

Description	Notation	Value
Diameter	D	40.5 m
Draft from MWL	H	198.2 m
Mass with entrapped water	M	$2.59 \cdot 10^8$ kg
MWL to center of gravity	Zcg	105.8 m
MWL to center of buoyancy	Zcb	99.1 m
MWL to mooring connection	Zf	105.6 m
Radius of gyration to MWL	Kr	122.8 m
Horizontal mooring stiffness	K	191 kN/m
Location of gauge above MWL	Zm	54.8 m
Water depth	D	922 m

Table 3.1 *Characteristics of test spar buoy*

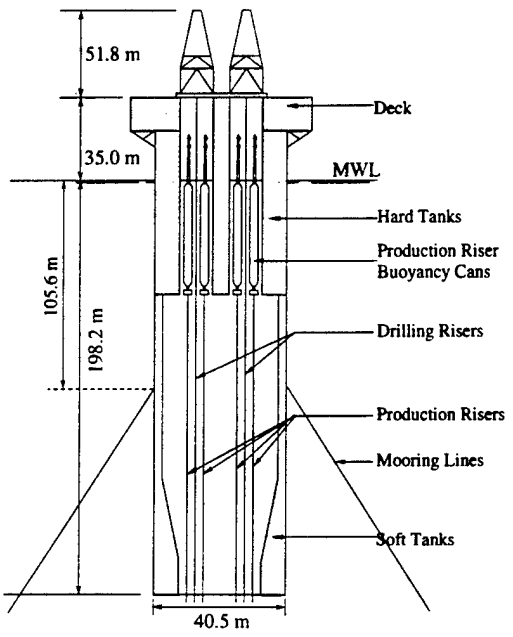

Fig 3.1 *Cross section of a spar buoy*

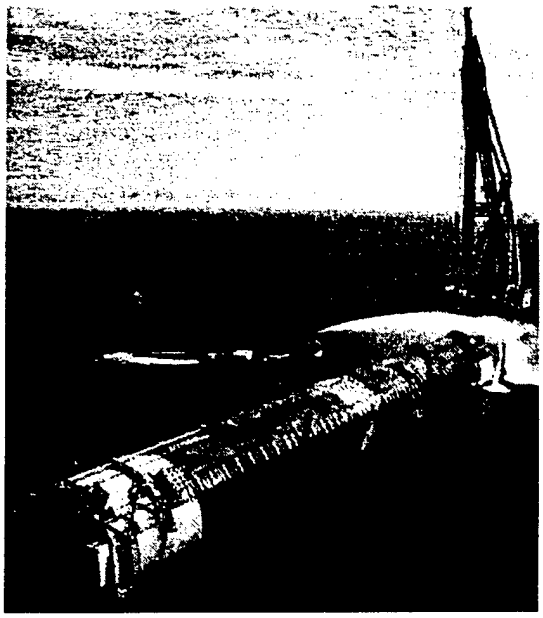

Fig 3.2 *Installation of the Neptune spar buoy*

Test	GOM1
Npts	9702
Nominal Hs (m)	13.1
Nominal Tp (s)	14.0
Observed Hs (m)	14.2
Observed Tp (s)	14.1
Calculated Tz (s)	10.8
Mean (m)	0.06
Standard deviation (m)	3.54
Skewness	0.31
Kurtosis	3.06
Minimum (m)	-9.05
Maximum (m)	12.74

Table 3.2 *Characteristics of test sea state*

The Data

Fourier Spectrum

The Fourier spectrum of the total response (figure 3.3) shows 3 distinct peaks, at 0.003, 0.015, and 0.07 Hz. These peaks correspond respectively to the natural periods in surge and pitch, and to the spectral peak period of the sea state (330s, 67s, 14s). All the wave energy is at the frequencies around the spectral peak period, where the response is related approximately linearly to the waves. Although there is no wave energy at the two low frequency peaks for surge and pitch, the system is excited at its natural frequencies by difference frequencies in the waves. This is the result of a non-linear forcing mechanism, which is discussed in detail by e.g. Faltinsen et al. (1990).

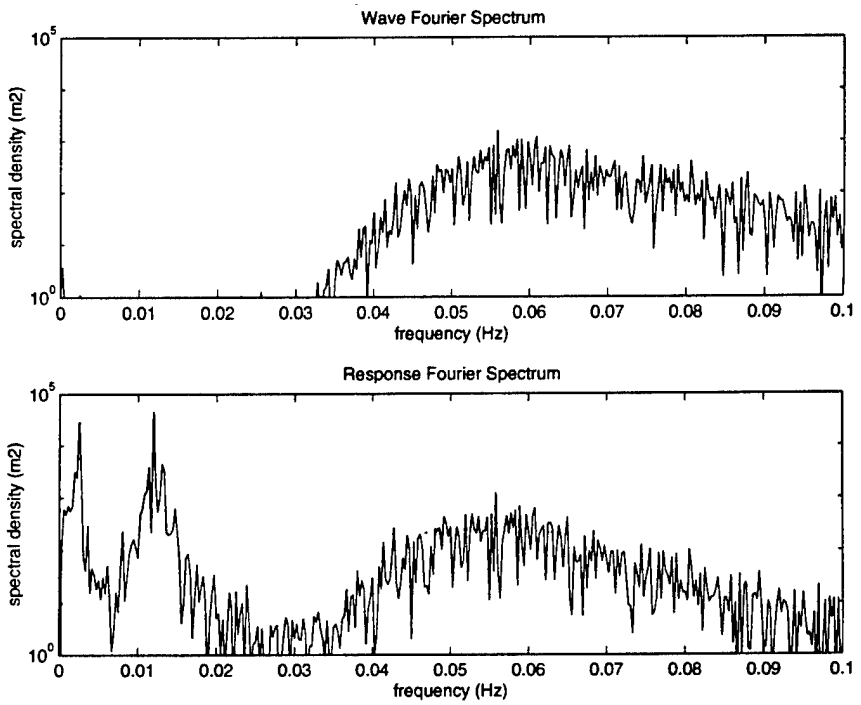

Fig 3.3 *Wave and response Fourier spectra for GOM1*

Time Series

In order to analyze the data, the response time series was filtered into 3 different components, surge, pitch, and wave frequency response, by simply introducing frequency cutoffs at 0.006 and 0.03 Hz. The filtered time series for the 3 components and the total are plotted in figure 3.4. For the selected location of the observed motions, the 3 components are of almost equal magnitude (7-9 m). Also note that in surge there are on average only 11 peaks per hour, while in pitch there will be 54 peaks on average. The limited amount of data of the extremes will affect the predictions we intend to make further on in this report. There have been discussions suggesting transient effects or "mode swapping" in the time trace of the total response. The observed behavior in this test, however, was found to be statistically consistent with one-hour segments of simulated steady state response to stationary random seas.

Moments

The moments of the process and the peaks are given in table 3.3. The mean of the components by definition is zero, due to the filtering operation. The mean total offset is almost 5 m, and has been removed for all the analyses. Also note that in particular for surge peaks, these moments are estimated from very few numbers, and are therefore "noisy". The limited amount of data can also bias the higher moments downward.

The base case we will refer to is a Gaussian process, for which the probability distribution of the continuous time trace will be normal. For a normal distribution the mean and standard deviation determine the distribution.

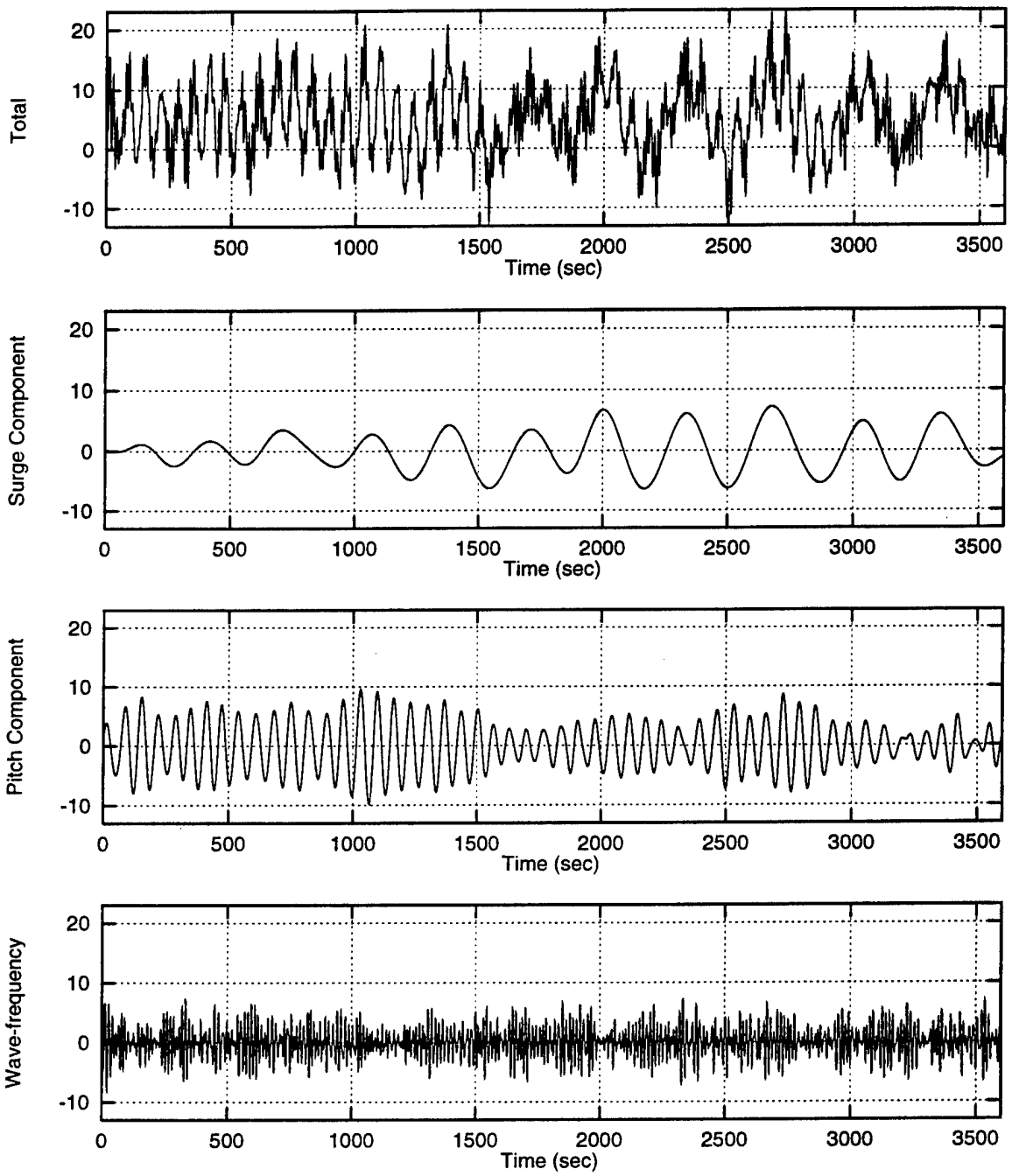

Fig. 3.4 *Time series of the total response and its major frequency components for GOM1*

The higher moments, the skewness and kurtosis, are implicit in the normal distribution. Their values are respectively 0 and 3. In contrast, the columns denoted m3 and m4 in table 3.3 report sample skewness and kurtosis values, estimated as in Eqs. 2.7-2.8. From these values, one may be tempted to infer that the responses show narrower than Gaussian distributions: although the skewness values of the process, reported in table 3.3, are nearly 0, the kurtosis values are systematically less than 3. We should note, however, that these low values of the kurtosis may be due, at least in part, to the effect of limited data. This lack of data will commonly lead to systematic underestimation of kurtosis values. Note, also, that the smallest estimated kurtosis values (2.17 and 2.20) are associated with pitch and surge, for which fewer independent cycles of motion are available.

Process	mean	stdv	m3	m4
Surge	0.00	3.37	0.10	2.20
Pitch	0.00	4.00	-0.01	2.17
Wave fr.	0.00	2.47	-0.03	2.70
Total	4.94	5.79	0.08	2.68

Peaks	mean	stdv	m3	CoV
Surge	4.39	1.93	-0.14	0.44
Pitch	5.26	2.02	-0.03	0.38
Wave fr.	3.11	1.55	0.29	0.50
Total	5.71	4.41	0.76	0.77

Table 3.3 *Moments of the response processes and their local peaks*

Alternatively, of course, these apparent narrower-than-Gaussian statistics may be due to some physical hardening mechanism, such as wave drift damping or perhaps non-linearity in the mooring forces. These two hypotheses (statistically biased moments due to limited data, vs. true hardening behavior) will be considered further in chapter 4,

which uses long simulated histories from a theoretical spar buoy response model to quantify the bias due to limited data.

As noted in chapter 2, if the time trace of the process is a narrow banded Gaussian process, its peaks will follow a Rayleigh distribution. The Rayleigh distribution of peaks corresponsing to a general normal process is given below, where μ_x represents the mean of the process, and σ_x the standard deviation of the process.

$$F_Y(y) = 1 - e^{-\frac{1}{2}\left(\frac{y-\mu_x}{\sigma_x}\right)^2} \qquad y \geq \mu_x \qquad 1.3$$

The Rayleigh distribution represents a special case of the Weibull distribution (Eq. 2.12), where the exponent, α is equal to 2, β is equal to $\sigma_x\sqrt{2}$, and $y = \mu_x$. The coefficient of variation of the peaks implicit in the Rayleigh distribution when $\mu_x = 0$ is equal to 0.5228 (Johnson & Kotz, 1970). The implicit skewness is 0.6311 (Johnson & Kotz, 1970). As noted in chapter 2, the kurtosis of the peaks contains little additional information here, as it is most useful for two-sided distributions, while the distribution of peaks is only one-sided (Kashef, 1998).

Table 3.3 shows that a Rayleigh model of peaks is most nearly consistent, in its CoV value (0.52), with the wave frequency response peaks. As the wave frequency response is physically thought to be a nearly linear transformation of the nearly Gaussian wave input, this result is not surprising. In contrast, surge and pitch results suggest somewhat narrower distributions, in terms of slightly lower CoV values and notably smaller

skewnesses than the Rayleigh model. Again, however, some of these effects may be due to the limited model test duration of 1 hour, which most severely impacts the statistics of surge and pitch components. In contrast, the peaks of the total process show a significantly higher CoV (0.77) than any of the components. As will be discussed further below, this arises due to the wide-band nature of the total response: its mixture of 3 frequency components leads, roughly speaking, to a mixture of Weibull distributions, with correspondingly larger CoVs.

The foregoing results at least suggest the need to include the potential for (1) non-Gaussian distributions of the process components; and (2) non-Rayleigh distributions of the response peaks. These are investigated in the next section, using both non-Gaussian (Hermite) process models and non-Rayleigh (Weibull and quadratic-Weibull) models of peaks.

Distribution of the Peaks

The 4 distribution models that were discussed in the previous chapter were fitted to the spar buoy data in order to study their applicability before predicting extreme values, which is our objective. The Hermite transformed Rayleigh and both Weibull distributions describe the distribution of local peaks and can be compared directly, although the Hermite model is fitted to the moments of the original process. The Gumbel distribution describes the global peaks and therefore cannot be compared directly to the other distributions of local peaks. The number of global peaks is selected by the user, and requires some insight in the data. In this case surge is the governing factor with the least

amount of peaks. Selecting more global peaks than there are local peaks would be inconsistent, as not all of the values in the set of 'selected peaks' will be real or local peaks. We selected the 10-minute global peaks for all time series, which gives 6 peaks per hour as a compromise between obtaining meaningful global peaks and a sufficient amount of data. The results were somewhat sensitive to the amount of global peaks. It turns out however that this effect disappears if we have multiple hours of data (see section 4.4).

Distribution Plots

The slope of the local peak data, when plotted on Weibull, scale is equal to the exponent α. The coefficient of variation can be estimated roughly by $1/\alpha$. The slope of data on Weibull-scale gives us an impression of how nearly the data follow a Rayleigh model ($\alpha \approx 2$). The slope of the data on Gumbel-scale is equal to $-\alpha$, which controls the standard deviation of the Gumbel distribution in an inverse way. In particular, the standard deviation of the Gumbel model equals $1.282/\alpha$. Curvature on either scale suggests the effect of higher moments is important to capture.

Local Peaks

The distributions of local peaks are shown in Figures 3.5-3.8. A first observation is that if we exclude the case of the total response (Figure 3.8), local peak data in the remaining three cases show no significant curvature on these Weibull scale plots. Hence, a Weibull model appears to suffice for all three components —surge, pitch, and wave frequency response. The higher-moment models (quadratic Weibull, Hermite) lead to no significant

difference, and do not appear in these cases to be worth the additional parameter(s) they require to fit. Among these three components, the Weibull models of both surge and wave-frequency response have slopes α near 2 (see Table 3.4), hence a still simpler Rayleigh model may suffice in these cases. The pitch component shows a narrower-than-Rayleigh distribution, with alpha nearly doubled (3.7), so that the best Weibull model provides a notable improvement over the Rayleigh in this case.

Weibull	mean	stdv	α	β
Surge	4.27	2.16	2.07	4.82
Pitch	5.80	1.75	3.69	6.43
Total	5.99	4.67	1.29	6.48
Wave fr.	3.09	1.57	2.07	3.49

Q Weibull	xmin	κ	β	$1/\alpha$	ε
Surge	-1.34	8.88	1.13	0.48	-0.81
Pitch	-0.29	6.27	1.11	0.27	-0.03
Total	-1.85	12.66	1.08	0.77	-0.73
Wave fr.	-0.55	4.59	1.13	0.48	-0.28

Hermite	mean	stdv *κ	c3	c4
Surge	-0.11	3.26	0.03	-0.06
Pitch	0.01	3.99	-0.01	-0.12
Total	4.84	5.94	0.02	-0.02
Wave fr.	0.00	2.46	0.00	-0.02

Table 3.4 *Distribution parameters*

Finally, we consider the total response peaks (Figure 3.8), which are the quantities of ultimate interest. Here the data itself does not convincingly follow a single Weibull model (i.e., appear to plot linearly) throughout its entire range. It might appear that a tail-fit Weibull model (e.g., to above 9 m) would lead to a somewhat steeper line (narrower distribution) than the moment-fit Weibull model shown in the figure. To explain this, it is

useful to recall that the Rayleigh model, and its Weibull generalizations, were postulated originally as models of peaks of relatively narrow-band processes.

We may expect this narrow-band assumption to be fairly accurate for each of the three component processes. The total response, however, represents a mixture of these three components, notable in view of (1) their very different time scales and (2) their similar contributions to the total variance of the process (Table 3.3). The resulting process will be far from narrow-banded, and its peaks may, roughly speaking, be considered as some type of mixture of Weibull distributions. In such cases, it may be difficult to expect a single, moment-fit Weibull to accurately track the distribution of peaks far into its upper tail. The added flexibility of the quadratic Weibull may prove useful in this case. Note too that the Hermite model can be argued to be an adequate model in the upper part of the distribution, though it far overestimates peaks at lower fractile levels. This is not accidental. Recall that the Hermite model does not sample the actual peaks at all; it merely samples moments of the non-Gaussian process, and creates a consistent narrow-band process by transforming a Rayleigh model of peaks. Because the total response is in fact wide-band, the narrow-band Hermite model cannot (and does not seek to) follow the peak distribution throughout its entire body. Because the effect of bandwidth becomes lessened for high response peaks, however, it may still be hoped that the Hermite model remains adequate for rare peak levels of practical interest. (This will again be taken up in Chapter 4, where additional data better illustrate the differences among these distributions of total response peaks.)

10-minute Global Peaks

Finally, Figures 3.9 and 3.10 show the observed distribution of global peaks: i.e., the 6 10-minute maxima in the 1-hour history. These figures are plotted on Gumbel scale; also shown in each case is the straight line arising from a Gumbel fit to the mean and standard deviation of these 6 maxima. With 6 data here, there is little chance to assess deviations from the Gumbel model. What is clear, however, is that the 10-minute maxima from the wave frequency response (upper half of Fig 3.10) show considerably less variability (higher slope) than all other cases.

In other words, once we compare global maximum responses over the same interval (here, 10 minutes), quantities involving slow drift motions (pitch, surge, and total response) show greater variability than those due to wave-frequency motions. This is due in part to the far fewer cycles of slow drift motion, and also to the light damping which induces high correlation among peaks (see table 3.5). Note, for example, the episodic, slowly evolving nature of the surge component of this model test, as shown in Figure 3.4. It is not difficult to imagine that its 10-minute extremes will show far more scatter than those, for example, of the wave-frequency response shown in the same figure. The net impact of this, as we shall see in following sections, is that we will generally require longer data sets to accurately estimate extremes of slow-drift motions, as compared with cases of wave-frequency motion alone.

Peaks:	global	local
Surge	0.33	0.50
Pitch	-0.07	0.69
Total	-0.13	0.03
Wave fr.	0.00	0.35

Table 3.5 Correlation coefficients of subsequent local peaks

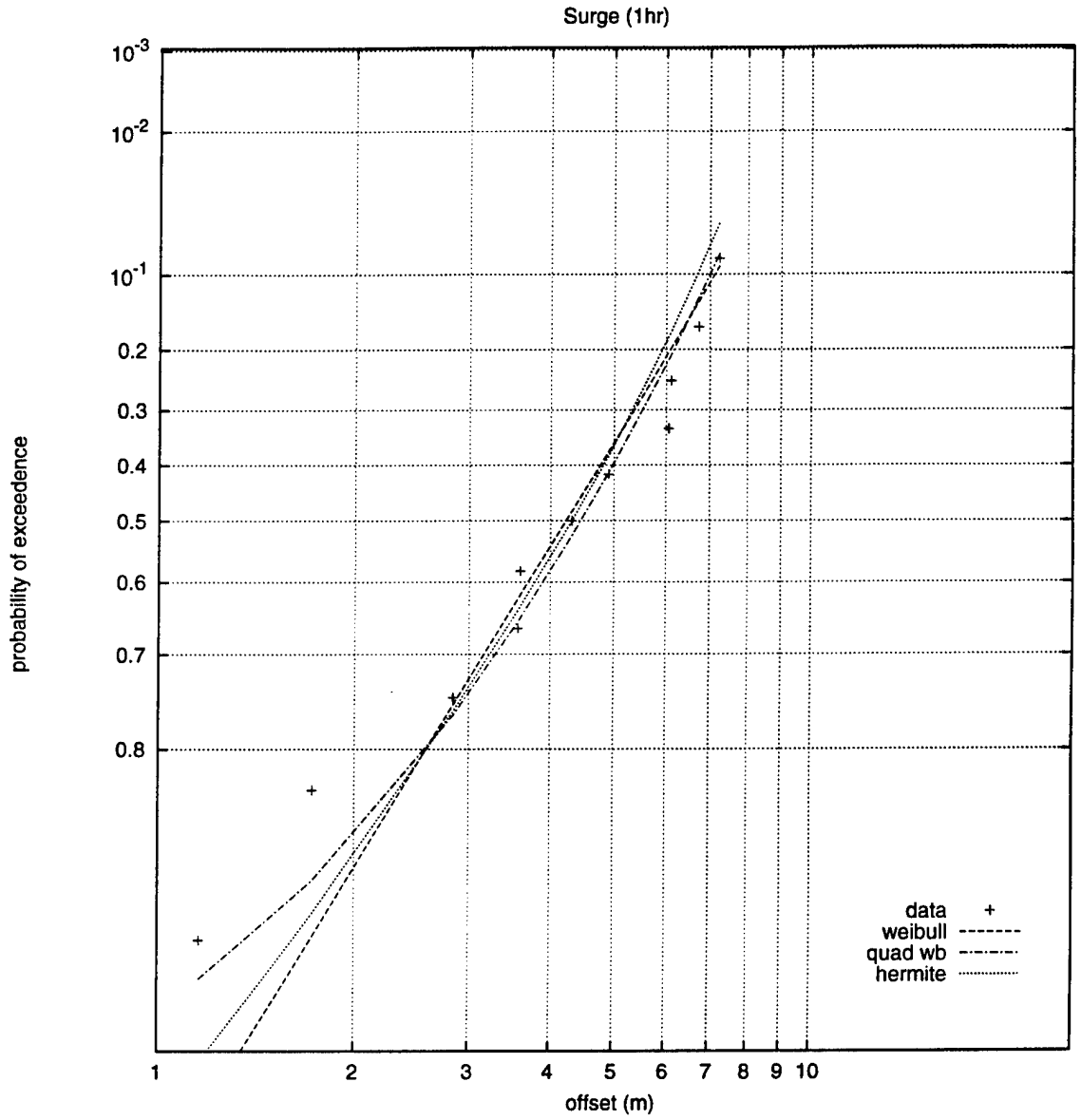

Fig 3.5 *Surge data and fitted distributions plotted on Weibull-scale*

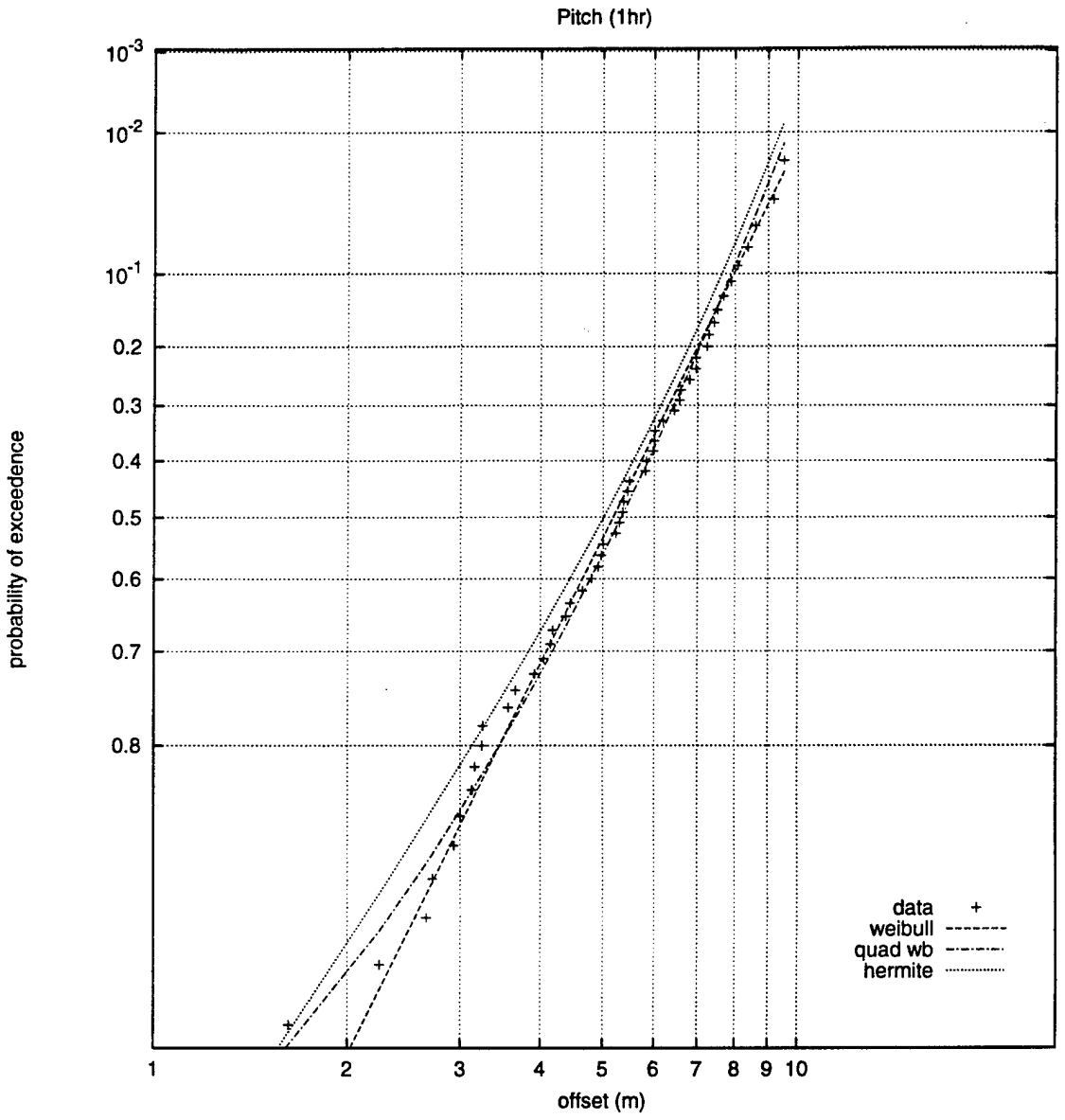

Fig 3.6 *Pitch data and fitted distributions plotted on Weibull-scale*

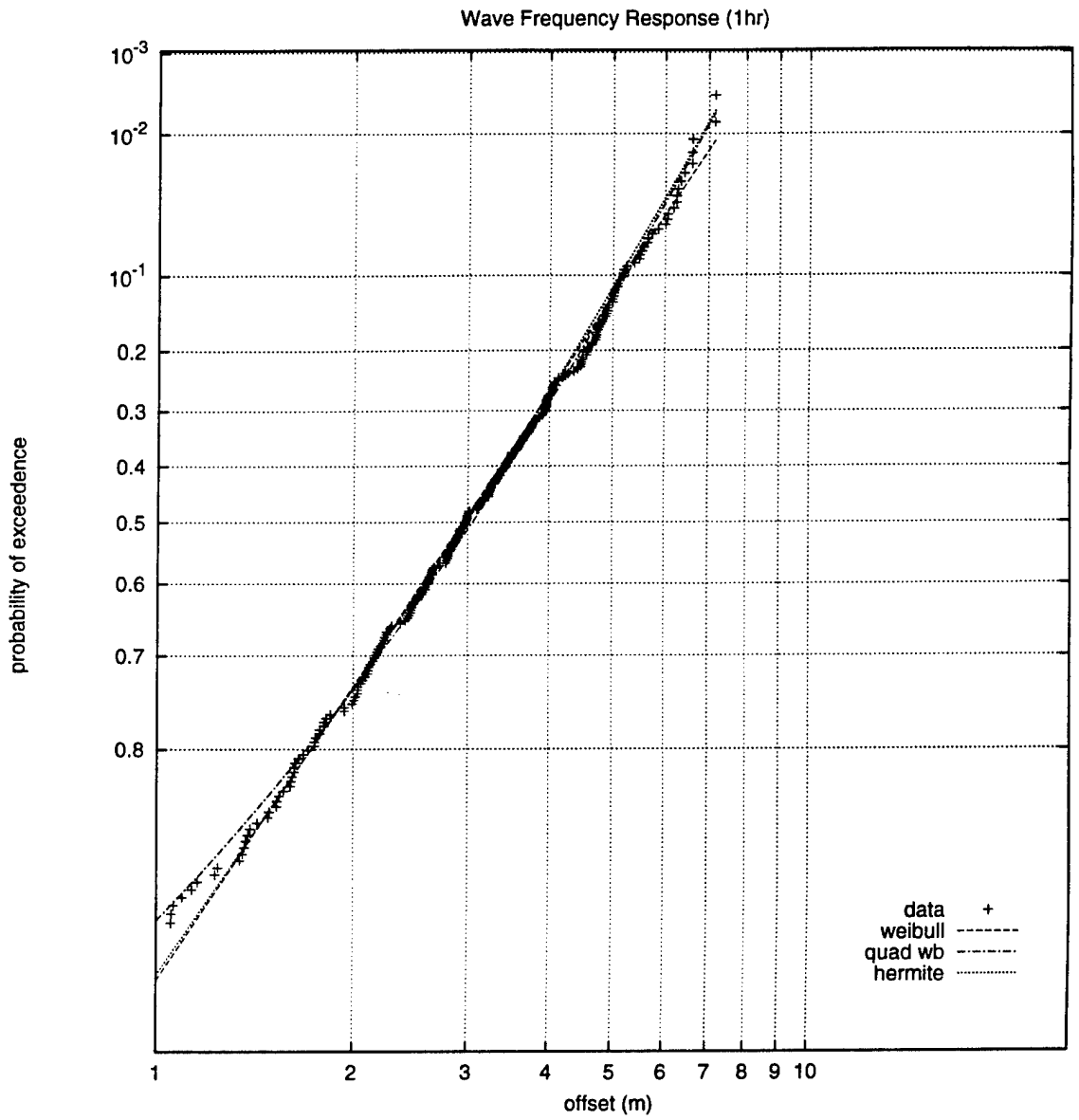

Fig 3.7 *Wave frequency response data and fitted distributions plotted on Weibull-scale*

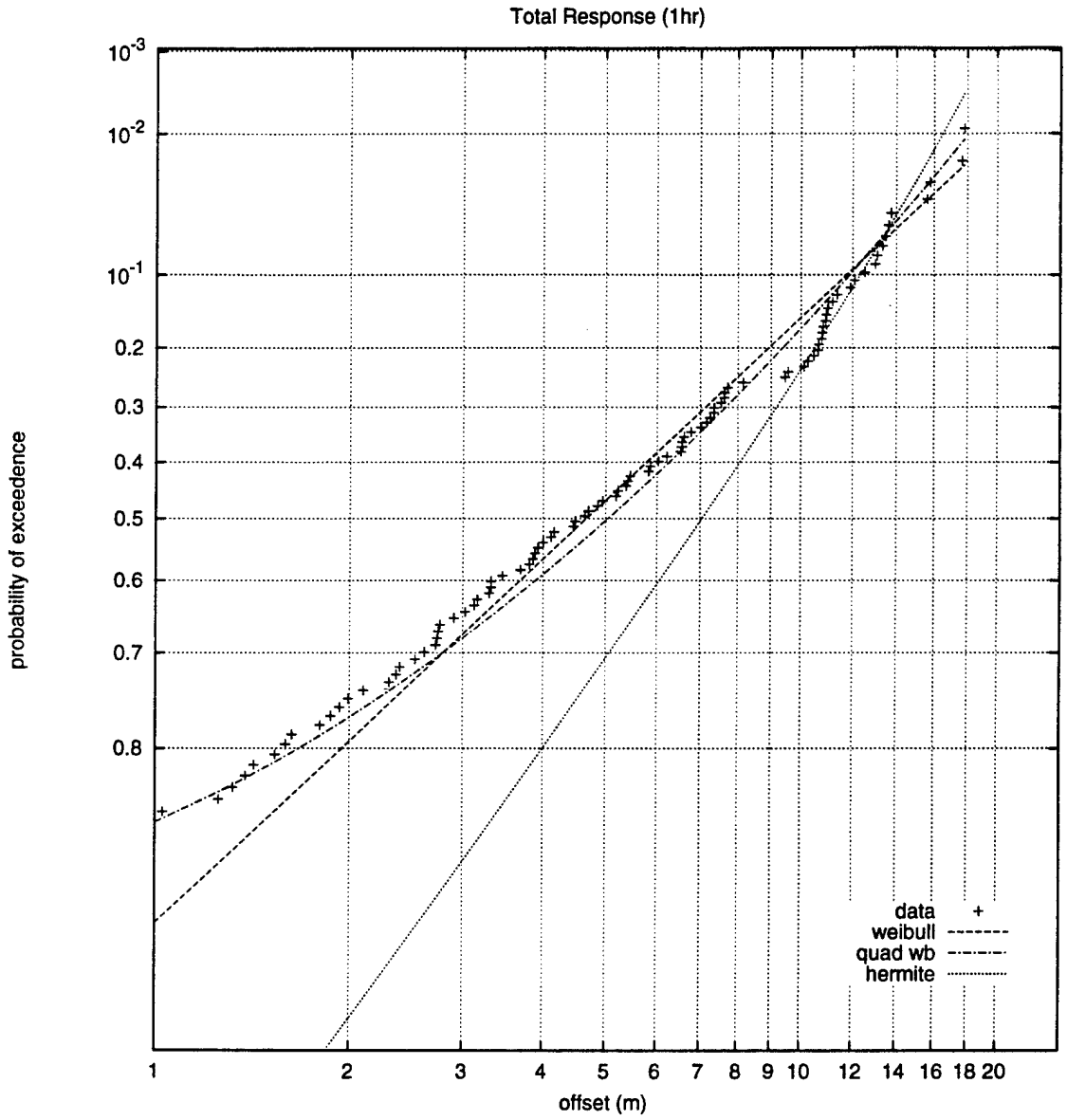

Fig 3.8 *Total response data and fitted distributions plotted on Weibull-scale (Note different horizontal scale from components)*

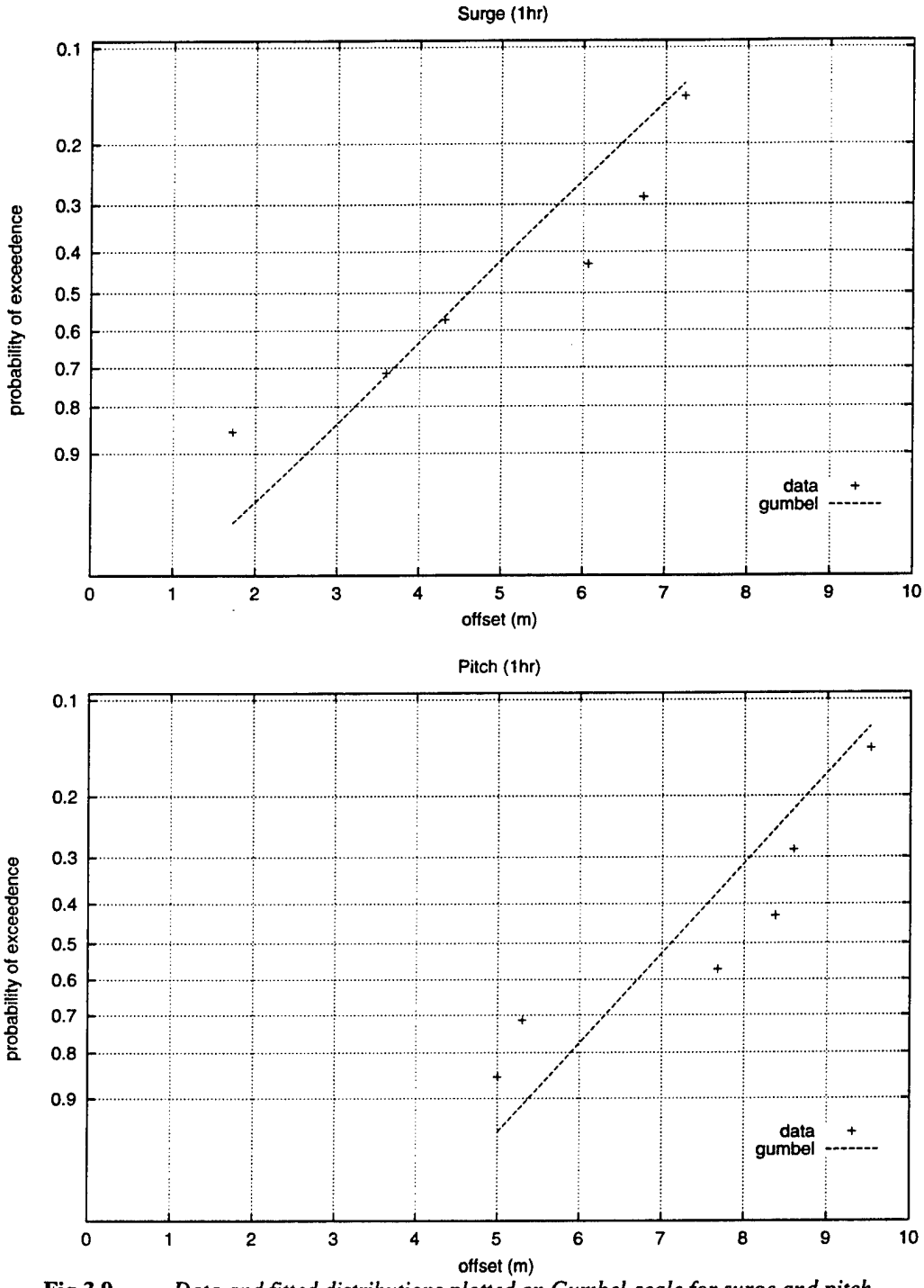

Fig 3.9 *Data and fitted distributions plotted on Gumbel-scale for surge and pitch*

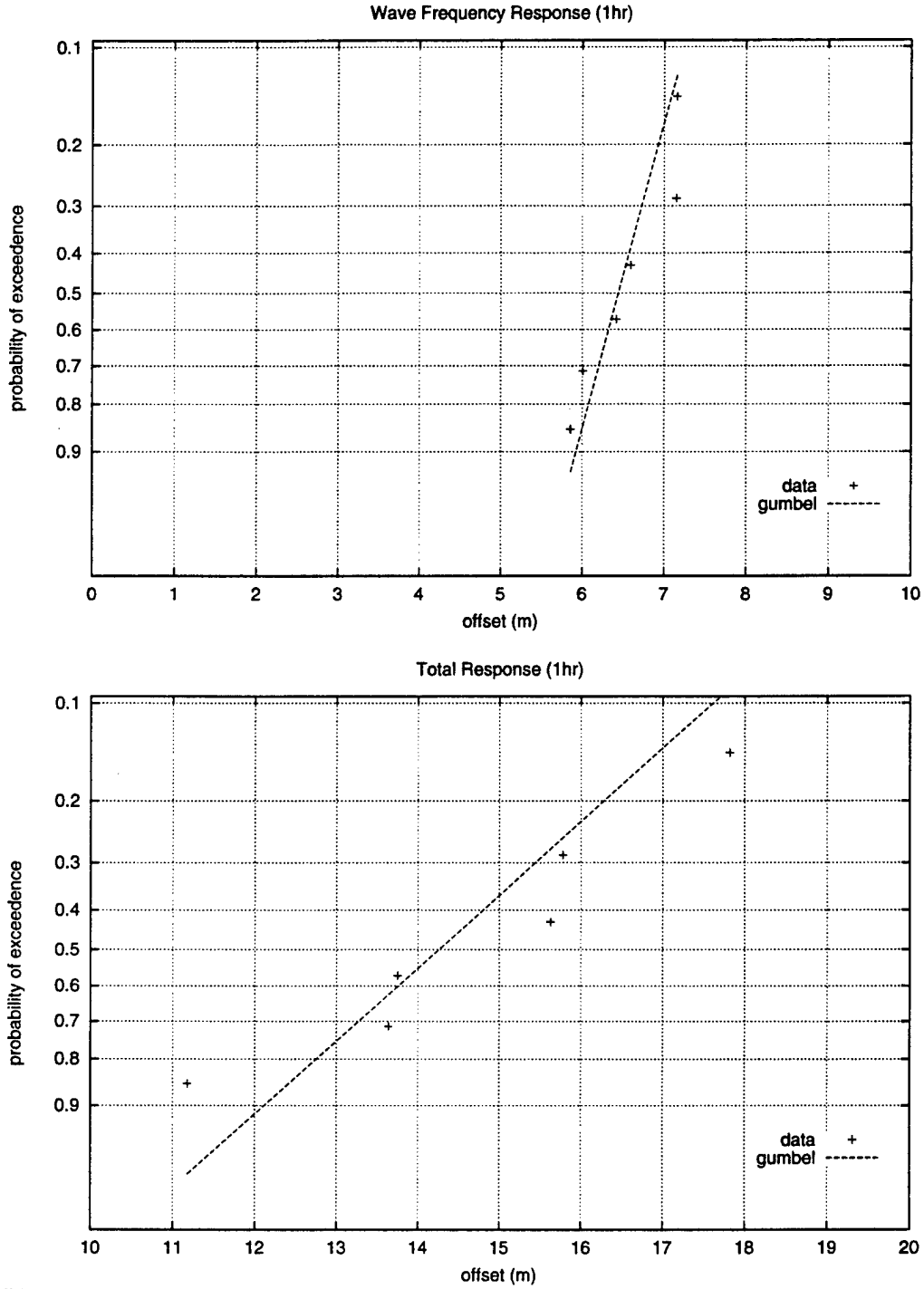

Fig 3.10 *Data and fitted distributions plotted on Gumbel-scale for the total and wave frequency response*

Estimating Statistics of the Extreme Value Distribution

This section discusses how we use the foregoing results to estimate the quantity of ultimate interest; namely, statistics of the distribution of X_{max}, the extreme response to occur in an arbitrary 1-hour duration.

As noted earlier, a first quantity of interest is μ_{Xmax}, the average value of X_{max} to be expected in an arbitrary hour. From the single hour of model tests, μ_{Xmax} can be directly estimated by the observed maximum value in that hour. (This will of course be quite a "noisy" estimate, but it will at least be unbiased.) Table 3.6 shows these direct estimates of the mean max, for each component and the total response, in the row marked "Observed". Other entries in the columns "Mean max" give estimates based on fitting one of the foregoing models (Hermite of process, Weibull or quadratic Weibull of local peaks, Gumbel model of 10-minute peaks) to the hour of data. To do this, note that each model first estimates the distribution function of X_{max}, based on either the distribution function of Y or Z (as in Eq. 1.6). The mean value of X_{max} is then estimated from its distribution function by numerical quadrature methods.

Surge

GOM1	Mean max	Bs_Stdv	CoV	# peaks
Observed	7.24	0.46	0.064	11
Gumbel	7.93	0.89	0.113	6
Weibull	7.88	0.77	0.097	11
Q Weibull	7.54	0.65	0.086	11
Hermite	7.16	-	-	11

Wave Frequency Response

GOM1	Mean max	Bs_Stdv	CoV	# peaks
Observed	7.16	0.17	0.024	265
Gumbel	7.31	0.29	0.040	6
Weibull	8.32	0.30	0.036	265
Q Weibull	7.66	0.27	0.035	265
Hermite	7.62	-	-	265

Pitch

GOM1	Mean max	Bs_Stdv	CoV	# peaks
Observed	9.52	0.33	0.035	54
Gumbel	10.03	0.59	0.059	6
Weibull	10.12	0.55	0.054	54
Q Weibull	9.59	0.46	0.048	54
Hermite	9.31	-	-	54

Total Response

GOM1	Mean max	Bs_Stdv	CoV	# peaks
Observed	17.82	0.72	0.040	112
Gumbel	17.86	0.91	0.051	6
Weibull	22.30	1.41	0.063	112
Q Weibull	19.49	1.10	0.057	112
Hermite	17.34	-	-	112

Table 3.6 *Mean hourly extremes for GOM1*

Bias

In principle, the bias associated with any model's estimate of μ_{Xmax} can be estimated from the ratio between its numerical estimate and the "Observed" unbiased value. As our observed value uses only a single observed extreme, however, we should not interpret these bias estimates too literally. It is somewhat encouraging, though, that most estimates lie within 10% of the observed values. The notable exception is the Weibull estimate for the total response, which exceeds the observed value by 25%. This perhaps supports the previous observation that since the total response shows three distinct spectral modes, its peaks are less well modeled by a single moment-fit Weibull model (as compared with the peaks of the relatively narrow-band component processes). This will be borne out in Chapter 4, in which the only significant bias results from applying the Weibull model to estimate extremes of the total response.

Uncertainty

In addition to seeking an estimate that is unbiased -- i.e., correct on average -- we also wish to consider the variability in the estimate due to limited data. In particular, we wish to determine whether fitting a model is useful in reducing variability in the estimated mean maximum μ_{Xmax}, as compared with using simply the observed maximum value.

As noted in Chapter 1, bootstrapping provides one method of estimating this variability. Its central idea is to create many synthetic, "equally likely" one-hour samples, by sampling from the observed data set with replacement. For example, the 1-hour surge component response is found here to have 11 local peaks (i.e., peaks above the mean response level). As shown in Table 3.6, a Weibull model applied to these 11 data yields the estimate of $\mu_{Xmax} = 7.88$m. Bootstrapping methods then suggest that this estimate has a standard deviation of 0.77m, and hence a CoV of .097 (the columns marked "Bs_Stdv" and "CoV" in Table 3.6).

To understand the bootstrap process used here, imagine that we have an 11-sided die, with each of the 11 local peak values written on one of its faces. We then imagine independently rolling this die 11 times. The resulting 11 outcomes are regarded as a new "bootstrap" sample. (Each of the outcomes must be a value of the original sample; moreover, it is almost inevitable that some values will arise multiple times, and other values omitted, from any particular sample.) We then repeat this exercise to create many bootstrap samples, and keep track of the estimates of μ_{Xmax} we find from each sample. The standard deviation of these estimates (here based on 200 bootstrap samples)

has been reported in Table 3.6. The quadratic Weibull model of surge is also based on all 11 of its peaks, hence its standard deviation is also found by creating new bootstrap samples of these 11 values. In contrast, the Gumbel model is based on an observed data set of only 6 10-minute maxima; these form the basis of new bootstrap samples (of size 6), to which the Gumbel estimator is repeatedly applied to assess its variability. (The standard deviation associated with the observed values of $\mu_{X_{max}}$ are found here by bootstrapping the entire vector of local peaks, again 11 in the case of surge, and then selecting the maximum of each bootstrap sample.)

In surveying the bootstrap-estimated CoV values in Table 3.6, one may note first that the observed estimates apparently show less variability than those produced by any of the corresponding models. If these results are truly representative, they would suggest that fitting these models is in fact disadvantageous. But in addition, the net CoV values seem unusually low, particularly those associated with the direct, observed estimates (e.g., only 2.4% in wave-frequency extreme, and 4% in pitch and total extremes). One may question whether these numbers are truly indicative of long-run behavior, or perhaps unusually low due to (1) the happenstance of the particular hour history chosen; or (2) some systematic uncertainty underestimation by the bootstrap method as currently implemented. Regarding point (2), our simple bootstrap sampling of response peaks neglects their correlation, which may well serve to underestimate the variability due to limited-duration samples. In addition, the bootstrapping method is in general tail-limited, failing to sample beyond the last data point observed, which may also affect extreme value estimation.

As in other issues raised in this chapter, distinction between issues (1) and (2) above requires a longer database of results, from which systematic trends can be distinguished from the particular values of this limited 1-hour test. This is the topic of Chapter 4.

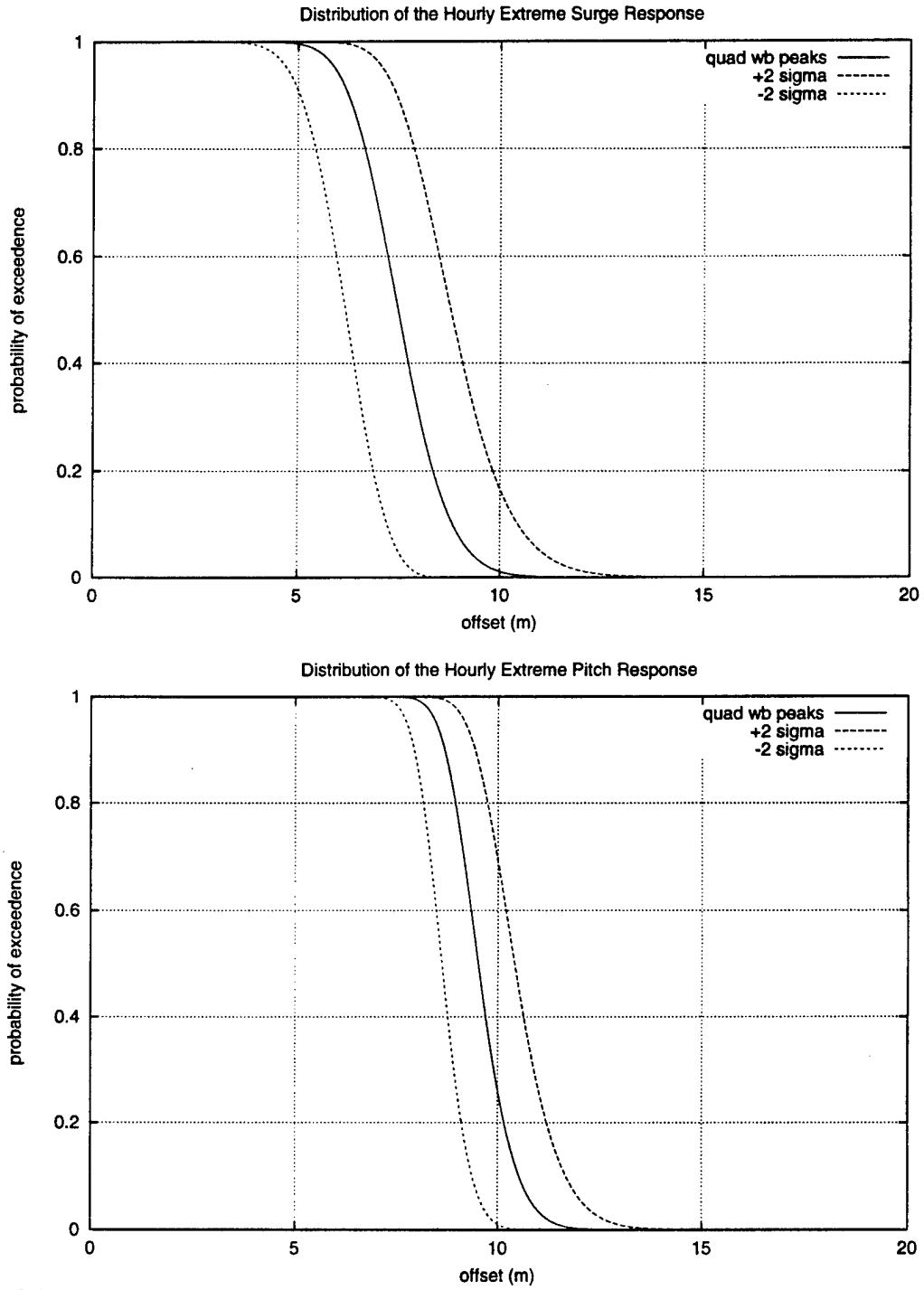

Fig 3.11 *Distribution of the predicted hourly extreme value for surge and pitch*

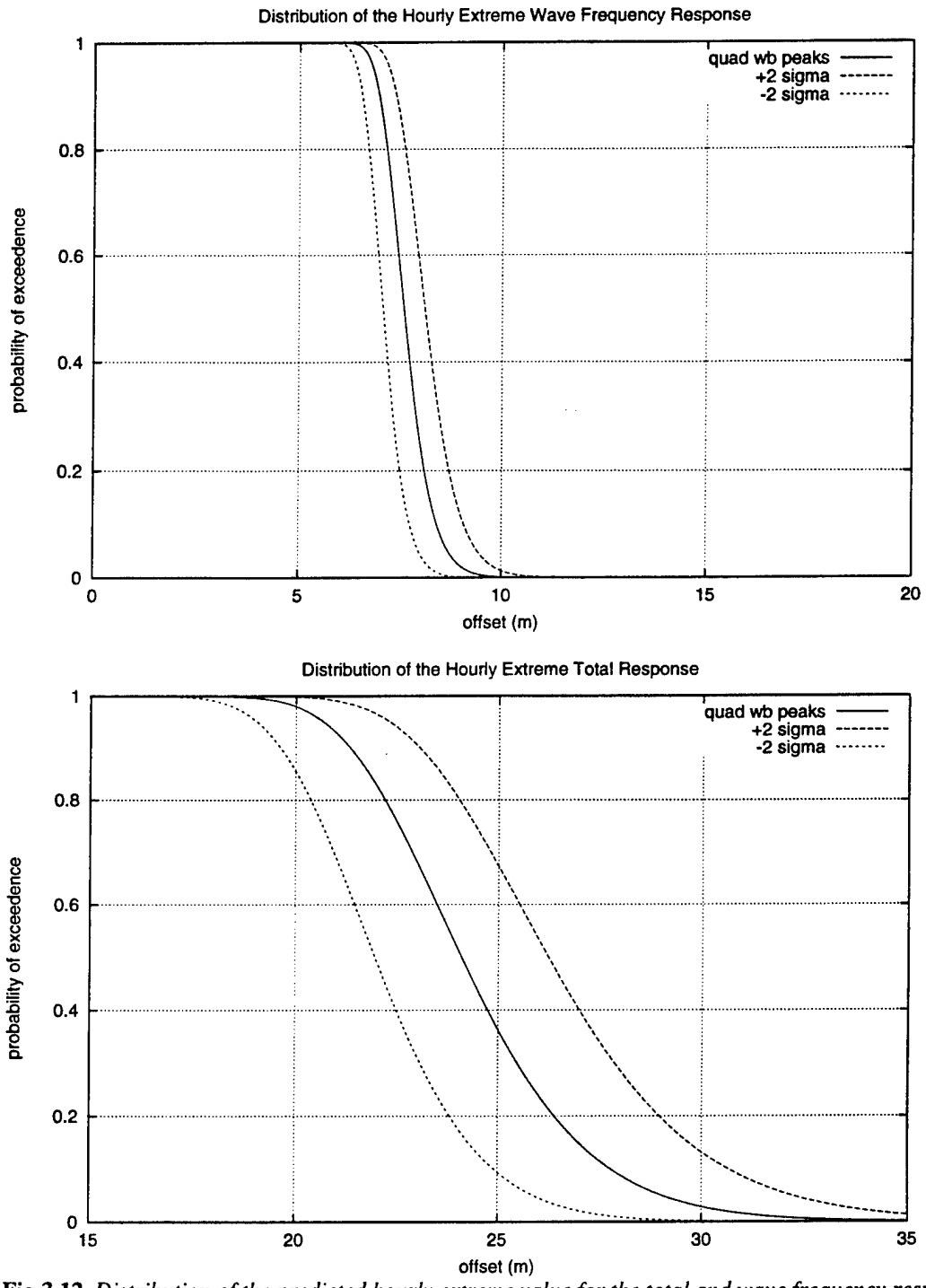

Fig 3.12 *Distribution of the predicted hourly extreme value for the total and wave frequency response*

SPAR BUOY RESULTS BASED ON 36 HRS OF DATA

Introduction

The results in the previous chapter are subject to a great deal of statistical uncertainty due to the very limited amount of suitable model test data that was available. The two main issues that emerged from chapter 3: "Are bootstrap estimates of the extreme statistics accurate?" and "Are the predictions of the distribution of extreme values made in chapter 3 biased?" will be revisited using an amount of data that intends to eliminate this uncertainty. In addition we will explore the answer to our original question "Does fitting a model, utilizing more of the original data, reduce the uncertainty in our predictions of the extreme values?" further.

In order to evaluate the results bootstrapping provided in the previous section, we seek to create multiple data sets by numerically simulating the model test, instead of resampling from the original data set. Although the model test that was analyzed was repeated once, the two hours of measured data do not provide a sufficient amount of data to improve the results of our analyses much. For the computer simulation we used the results from second order diffraction analysis, and post-processed these using a routine called "TFPOP" (Ude 1996). In fact this,simulation-based method may be regarded as a form of parametric bootstrapping as opposed to the non-parametric bootstrapping method used in the previous sections. The TFPOP-model for the OTRC spar buoy was developed and verified by Jha (1997).

Non-parametric bootstrapping may not be very useful to estimate the bias in our predictions of the mean extreme value, as all the data sets we compare are produced with the same, possibly biased estimator. Simulation however, does allow us to evaluate the bias in our predictions, as we are not assuming a statistical model that we are testing at the same time. In order to do this however we need to trust that the wave tank accurately reproduced the wave spectrum that was assumed for the calculations, and that the computational model provides accurate predictions of the response on a wave by wave basis. In other words: We have to assume that the model uncertainty added will not affect our results.

Computational Model

The model of the structural response (i.e. the horizontal offset at 54.8m) assumes a rigid body with 2 degrees of freedom (surge and pitch). The first- and second-order transfer functions were established by Kim and Yue (1989, 1991). These results were the basis of Jha's model, which includes additional effects, such as wave drift damping, viscous effects, mooring stiffness, etc. The final results consisted of 4 alternative models for the spar buoy.

1. Base-case model with diffraction forces
2. Model with diffraction forces and wave-drift damping
3. Model with diffraction forces, wave-drift damping and viscous force from undisturbed waves

4. Model with diffraction forces, wave-drift damping and viscous force from disturbed waves

Jha concludes that, together with diffraction forces, viscous effects should be included to accurately predict the mean offset of the spar. As the simulations do not provide us with the disturbed wave surface near the structure, the third model was selected. Fortunately the use of the disturbed wave surface showed no significant improvement of the results compared to the results based on the undisturbed wave surface (Jha, 1997).

For time domain simulation we have to solve the basic equation of motion in the time domain.

$$M\ddot{x}(t)+C\dot{x}(t)+Kx(t)=F(t) \qquad 4.1$$

Where:

x(t)	: horizontal offset at 54.8 m	C	: damping matrix
M	: mass matrix	K	: stiffness matrix
F(t)	: applied (hydrodynamic) force		

The hydrodynamic force is a function of the random wave process $\eta(t)$, the geometry of the structure, and the water depth.

Waves

The wave environment for the test is intended to represent the 100-year extreme significant wave height sea state for the Gulf of Mexico. A Jonswap spectrum with Hs = 13.1m, Tp = 14.0s, and a peakedness factor of 2.0 was used to represent these conditions. The model tests however showed an observed Hs of 14m, which was used in the computer simulations instead. From the wave spectrum complex Fourier amplitudes, $C(\omega_k)$ are simulated using:

$$C(\omega_k) = \sqrt{2S_x(\omega_k)\Delta\omega e^{i\theta_k}} \qquad 4.2$$

The phase angles θ_k, are selected random from a uniform distribution between 0 and 2π. The spectral amplitudes $S_x(\omega_k)$ are taken as exponentially distributed random variables with a mean value given by the wave spectrum at ω_k (Ude, 1996). These "noisy" simulations intend to reproduce Gaussian ensembles better than more straightforward deterministic methods. In addition "noisy" simulation tends to predict the variance of the second order response better (Ude, 1995).

The irregular waves can be written in the time domain as:

$$\eta(t) = \mathrm{Re}\sum C(\omega_k)\exp(i\omega_k t) \qquad 4.3$$

Although TFPOP uses linear waves as input, the transfer functions for the hydrodynamic forcing also add a second order Stokes component to the waves. Therefore effectively a second order random wave model was used.

Hydrodynamic Forcing Model

Diffraction analysis entails applying sinusoidal waves of different frequencies, ω_k, selected from the wave Fourier spectrum to a structure, as described in the previous paragraph to the structure. The first-order forces are then found at these incident wave frequencies as:

$$f_1(t) = \mathrm{Re} \sum C(\omega_k) H_1(\omega_k) \exp(i\omega_k t) \qquad 4.4$$

where H_1 is the first-order transfer function and the $C(\omega_j)$ coefficients are the complex Fourier amplitudes. The second-order forces are found at pairs of frequencies as:

$$f_2(t) = \mathrm{Re} \sum \sum C(\omega_m) C(\omega_n) H_2^-(\omega_m, \omega_n) \exp[i(\omega_m - \omega_n)t] \qquad 4.5$$

where H_2^- is referred to as the difference-frequency quadratic transfer function (QTF).

Note that in order to find these transfer functions the spar was allowed to float freely (Kim and Yue 1989, 1991). Linear diffraction analysis was used to estimate the frequency-dependent added mass and damping for the spar. The second-order diffraction analysis is computationally intensive and limited to a few frequency pairs (here 8x8

frequency grid ranging from 0.2 to 1.18 rad/s). A surface spline fitting scheme was used to interpolate the sparse QTF to finer mesh used by TFPOP (Jha, 1997).

The viscous forces are calculated with Morison's equation, integrated from the keel to the free surface. The drag force was based on the absolute fluid velocity with an assumed drag coefficient of 0.6:

$$f_D(x,z) = \rho R_D C_D u(x,z)|u(x,z)| \qquad 4.6$$

Wheeler stretching (Wheeler, 1970) was used to determine the velocity of the water particles above the mean water level, for which linear wave theory does not provide a solution.

Structural Model

The spar's horizontal offset in the wave direction consists of 2 components, a displacement in the wave direction, and a rotation in the plane of the waves, respectively its surge and pitch modes. The structure is modeled as a rigid body with 2 degrees of freedom, and the following mass, stiffness, and damping matrices. (The first mode is surge, while the second is pitch.)

$$M = M_{str} + M_{add} \qquad 4.7$$

where M_{str} is the total mass of the spar and the water entrapped in the center well, and M_{add} is the (frequency dependent) added mass matrix, reflecting the effects of waves radiated by the oscillating spar. The added mass was obtained from diffraction analysis, and is assumed to be constant for low-frequency modes.

$$M_{str} = \begin{bmatrix} m & -mZ_{CG} \\ -mZ_{CG} & I(=mK_r^2) \end{bmatrix} = \begin{bmatrix} 2.59 \cdot 10^8 kg & -2.74 \cdot 10^{10} kgm \\ -2.74 \cdot 10^{10} kgm & 3.91 \cdot 10^{12} kgm^2 \end{bmatrix} \quad 4.8$$

$$M_{add} = \begin{bmatrix} 2.71 \cdot 10^8 kg & -2.60 \cdot 10^{10} kgm \\ -2.60 \cdot 10^{10} kgm & 3.20 \cdot 10^{12} kgm^2 \end{bmatrix} \quad 4.9$$

The symbols are explained in table 3.1.

Note that M_{str} and M_{add} are of the same order of magnitude for this large-diameter structure.

The stiffness matrix, derived from geometry considerations is found to be:

$$K = \begin{bmatrix} k & -kZ_f \\ -kZ_f & kZ_f^2 + k_h \end{bmatrix} = \begin{bmatrix} 1.91 \cdot 10^5 Nm^{-1} & -2.02 \cdot 10^7 N \\ -2.02 \cdot 10^7 N & 1.60 \cdot 10^{10} Nm^{-1} \end{bmatrix} \quad 4.10$$

where:

$$k_h = \pi R^2 H \rho g (Z_{CG} - Z_{CB}) - \frac{\pi}{4} \rho g R^4 \qquad 4.11$$

The eigenfrequencies associated with these structural properties are 331 s in surge and 69.9 s in pitch, which correspond to the frequencies observed in the response Fourier spectrum and the free decay tests. The eigenmodes also confirm the model, as they show the correct geometric relation between surge and pitch (i.e. 1 unit of surge offset results in zero pitch rotation, and 1 radian pitch rotation results in 100.6 m surge offset).

What remains to be modeled is the damping of the structure, which is the most challenging part. From modal analysis we can construct the damping matrix C as follows:

$$\Phi^{-1} M^{-1} C \Phi = \begin{bmatrix} 2\zeta_s \omega_s & 0 \\ 0 & 2\zeta_p \omega_p \end{bmatrix} \qquad 4.12$$

where ω_s, and ω_p are the natural periods, and ζ_s, and ζ_p are the damping ratios in surge and pitch respectively. Φ represents the eigenmatrix.

The damping ratios were used to calibrate the model to the observed response. This was done in an iterative procedure to match the bandwidth parameter, δ of the response Fourier spectrum.

$$\delta = \sqrt{1-\lambda_1^2\left(\lambda_{0\lambda_1}\right)} \qquad \lambda_n = \int f^n S(f) df \qquad 4.13$$

where:

λ_n : the n^{th} spectral moment S(f) : spectral density at frequency f

Alternative methods and pitfalls are discussed by Jha (1997). In addition we may account for wave drift damping. Although wave drift damping does not represent a physical loss of energy, it is also an effect that is proportional to the structure's velocity. In principle it accounts for the structures relative velocity to the water. On the hydrodynamic forcing side of the basic equation of motion there will be a term proportional to the velocity of the water relative to the structure squared. This term is linearized, and the velocity of the structure is brought to the other side of the equation, where it is grouped with the damping terms. The calibrated values for ζ will therefore depend on whether we account for wave drift damping or not. In this case we do, which results in damping ratios of 4.0% and 0.5% in surge and pitch respectively. As wave drift damping is frequency dependent the elements of C are not reported here. The diagonal terms for wave drift damping were calculated using SWIM (MIT). The off-diagonal terms were estimated with Newman's approximation (Newman, 1974).

The Data

Using the model of the OTRC spar 36 hours of response data were simulated. Analogous to the previous chapter we will analyze the data, the distributions of peaks, and the distribution of the global extremes.

Moments

The moments of the process and the peaks are reported in table 4.1 for the total 36 hours.

Process	mean	stdv	m3	m4
Surge	0.00	3.95	-0.04	3.13
Pitch	0.00	3.83	-0.01	3.00
Wave fr.	0.00	2.61	0.00	2.97
Total	5.11	6.08	0.04	2.98

Peaks	mean	stdv	m3	CoV
Surge	4.83	2.67	0.65	0.55
Pitch	4.77	2.52	0.59	0.53
Wave fr.	3.26	1.72	0.57	0.53
Total	5.41	4.36	1.06	0.81

Table 4.1 *Moments of the process and its local peaks for 1x36 hrs of response data*

Contrary to the 1-hour results, the moments for the processes seem to be very Gaussian, with skewnesses near zero and kurtosises very close the 3. The peaks of each of the components also appear to be well modeled by Rayleigh distributions, with coefficients of variation close to 0.52, and skewnesses near 0.63. Only the local peaks of the total response, arising from cycles over 3 separate time scales, depart clearly from the Rayleigh model. This may be expected, as the total response no longer shows the narrow-band frequency content consistent with the Rayleigh model.

Besides the first-order wave frequency response, also surge and pitch, the second-order part of the system's response seem to be linear. There are various possible explanations for the Gaussian behavior during the simulation, compared to the model test, which does not seem Gaussian. The computer model assumes the moorings to behave as a linear spring, which is a crude approximation of reality, especially for large displacements. The moorings in the model test are not linear, and may cause a certain amount of non-Gaussianity. However, more importantly, the amount of data used (e.g. 390 peaks in surge) has eliminated most of the noise and bias, which was present in the results for a single hour of data. Table 4.2 reports the means of the 36 1-hour moments of he data set, which strongly suggest that using a limited 1-hour duration of data biases the skewness and kurtosis of the process and the skewness and the coefficient of variation of the local peaks.Although the moments are not as low as the moments of the single hour of observed data, which are reported in table 3.3, the limited amount of data explains a good deal of the bias. The higher moments of surge and pitch, which have the least amount of peaks, are affected most by the data reduction.

Process	mean	stdv	m3	m4
Surge	0.00	3.79	-0.01	2.59
Pitch	0.00	3.76	-0.01	2.63
Wave fr.	0.00	2.61	0.00	2.96
Total	5.11	6.02	0.05	2.87

Peaks	mean	stdv	m3	CoV
Surge	4.70	2.23	0.25	0.47
Pitch	4.76	2.28	0.25	0.48
Wave fr.	3.25	1.71	0.55	0.53
Total	5.50	4.34	0.95	0.79

Table 4.2; *Moments of the process and its local peaks for 36x1 hr of response data*

Distribution of Peaks

Distribution of Local Peaks

For practical reasons we cannot display the 36 1-hour distributions per component. Instead the models were fitted to the entire 36 hours of data (fig 4.1-4.4) The plotted distributions in fig 4.1-4.4, based on 36 hours of data, clearly show that if we restrict attention to any single component all of the models behave quite well. There is little advantage at the component level to generalize the Weibull through a quadratic transformation. When considering the total response however, the quantity of ultimate interest, differences between the models emerge.. The 'observed' distribution of the total shows a "corner" in the distribution around 17 m, which the standard Weibull fails to capture. The quadratic Weibull follows the data better near the T = 1 hr to 6 hr return period extremes, but it is not clear how the distribution behaves even further out in the tail. The Hermite model also appear to be able to capture the tail behavior above the "corner" well (i.e. for mean return periods of T = 1 to 6 hrs), but fails to capture the body of the distribution. Recall that the Hermite model here transforms a narrow-band Gaussian process (with Rayleigh peaks). Hence it does not accurately model –nor was it intended to model- the less interesting lower fractile peaks of a wide-band process. These results clearly suggest that fitting a distribution to the total response here should be done with care. In general problems might arise when a single limited-parameter model, such as the Weibull, is applied to cases where actual peaks arise from a mixture of different phenomena. Here, the mixture is due to response components with different tim-scales. In previous applications to jack-up forces and responses, the mixture arose from

the combination of drag- and inertia-induced effects. The Weibull model was found to show similar, though non-conservative errors in this case (Torhaug, 1996).

Distribution of 10-minute global peaks

The Gumbel model, applied to the 10-minute global peaks shows similar accuracy to the best of the preceding models (Hermite and quadratic Weibull) based on local peaks. In particular, fine agreement is found through the T = 1 hour return period response, even for the total response. Comparing the "total response" plots in Figs. 4.4 and 4.6, all models except the Weibull accurately predict the observed 1-hour response of about 18 m, while the Weibull model returns a 1-hour response of roughly 20m (i.e. about 10% error)

At or near the T = 6 hour mean return period, one may view Figs. 4.5-4.6 as suggesting that the Gumbel model becomes somewhat conservative. At the same time, one should be wary about inferences based on the last few data points. (In comparing Figs 4.1-4.4 with 4.5-4.6, one should note that the first two plot the offset, x, on log-scale, thereby visually deemphasising deviations in the upper-tails.)

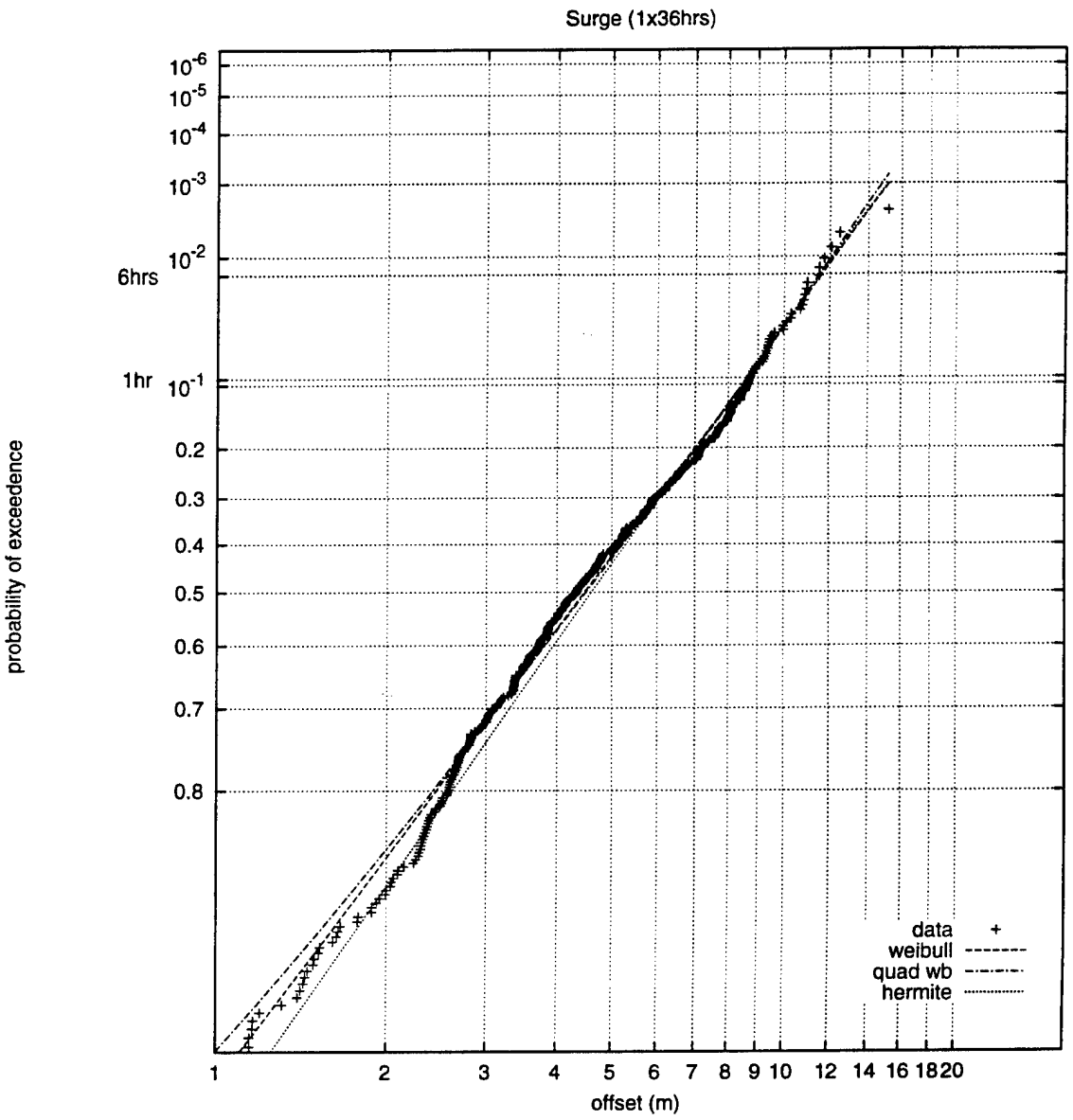

Figure 4.1: *Surge local peaks and fitted distributions plotted on Weibull-scale*

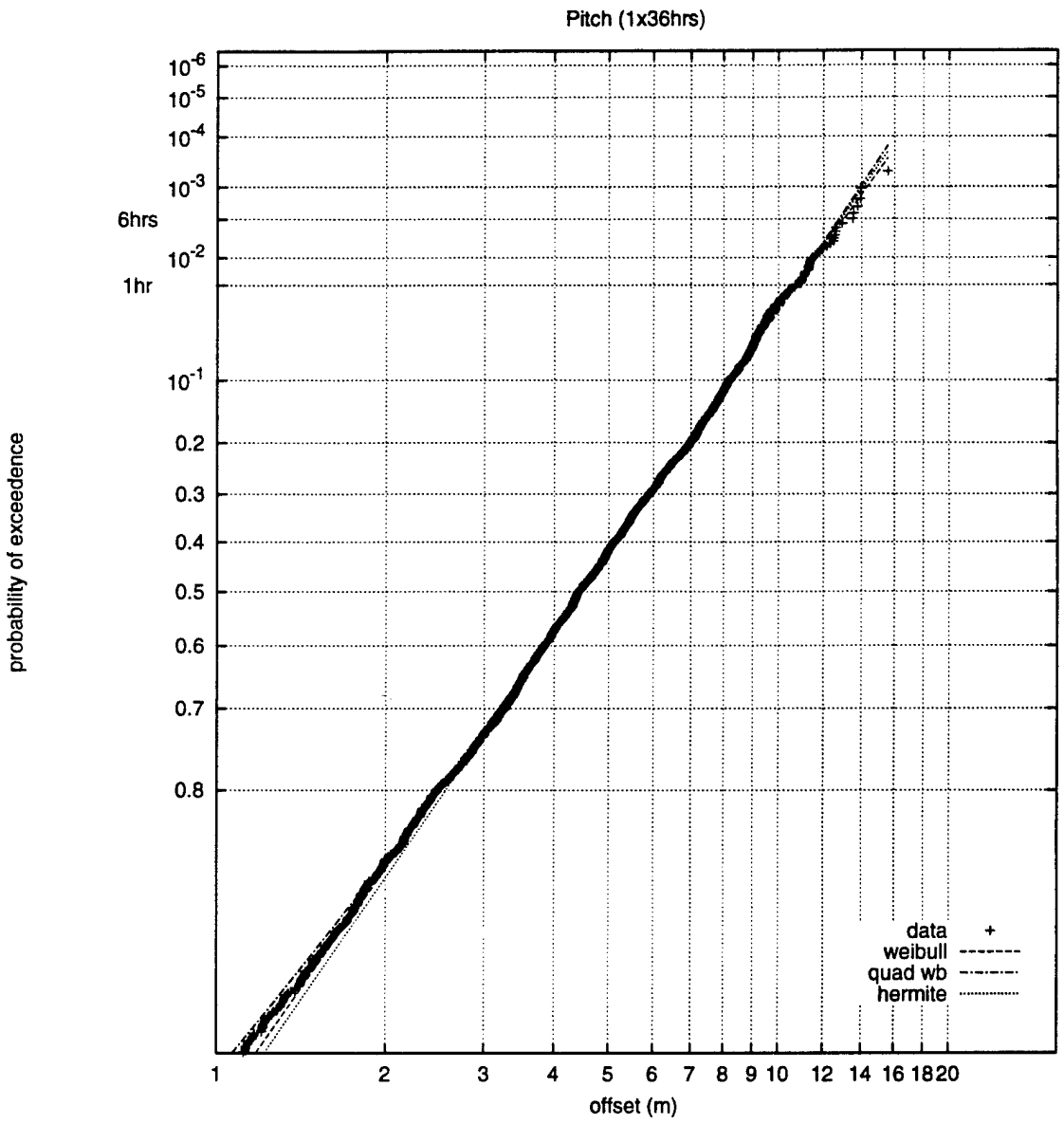

Figure 4.2: *Pitch local peaks and fitted distributions plotted on Weibull-scale*

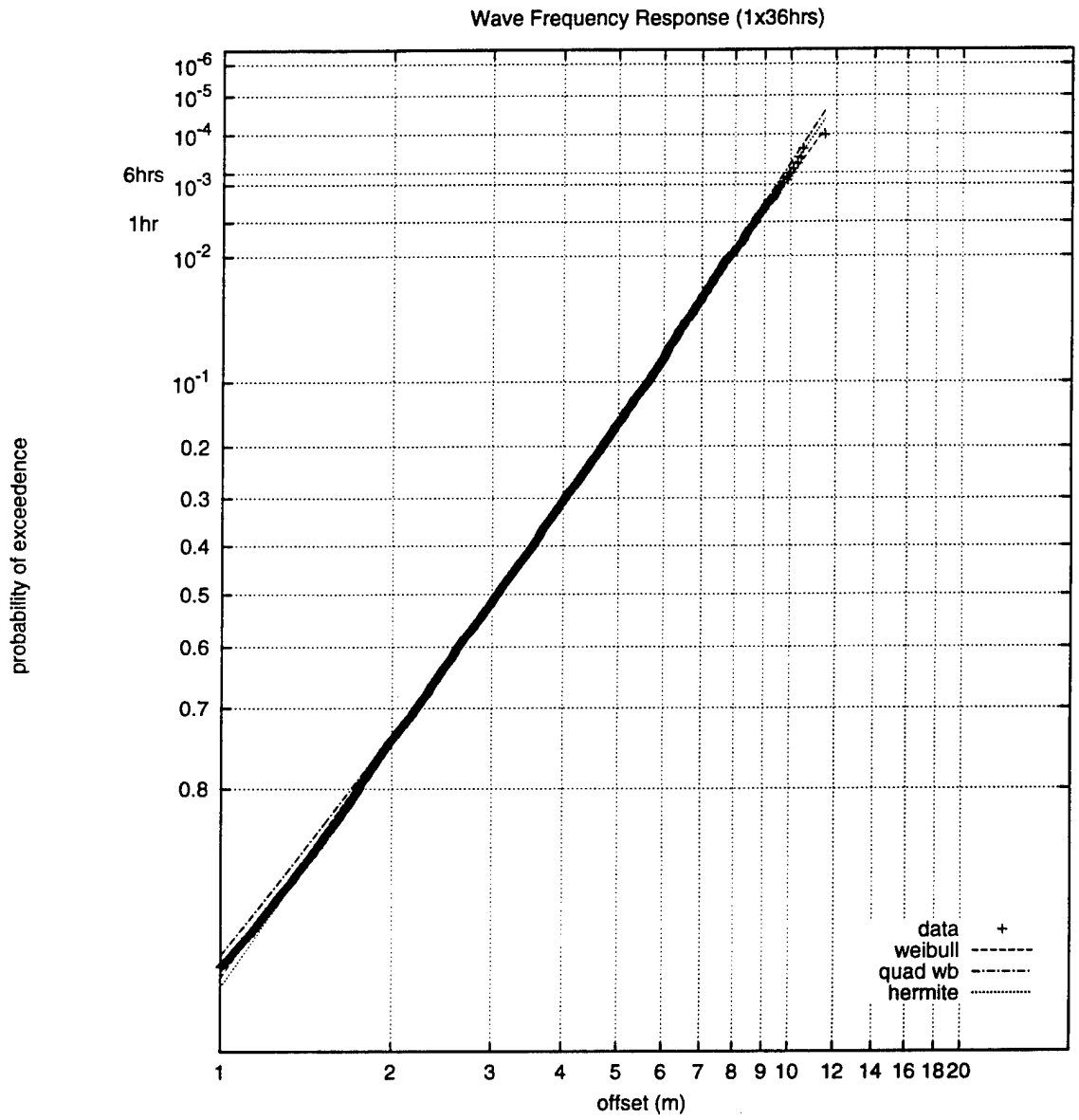

Figure 4.3: *Wave frequency response local peaks and fitted distributions plotted on Weibull-scale*

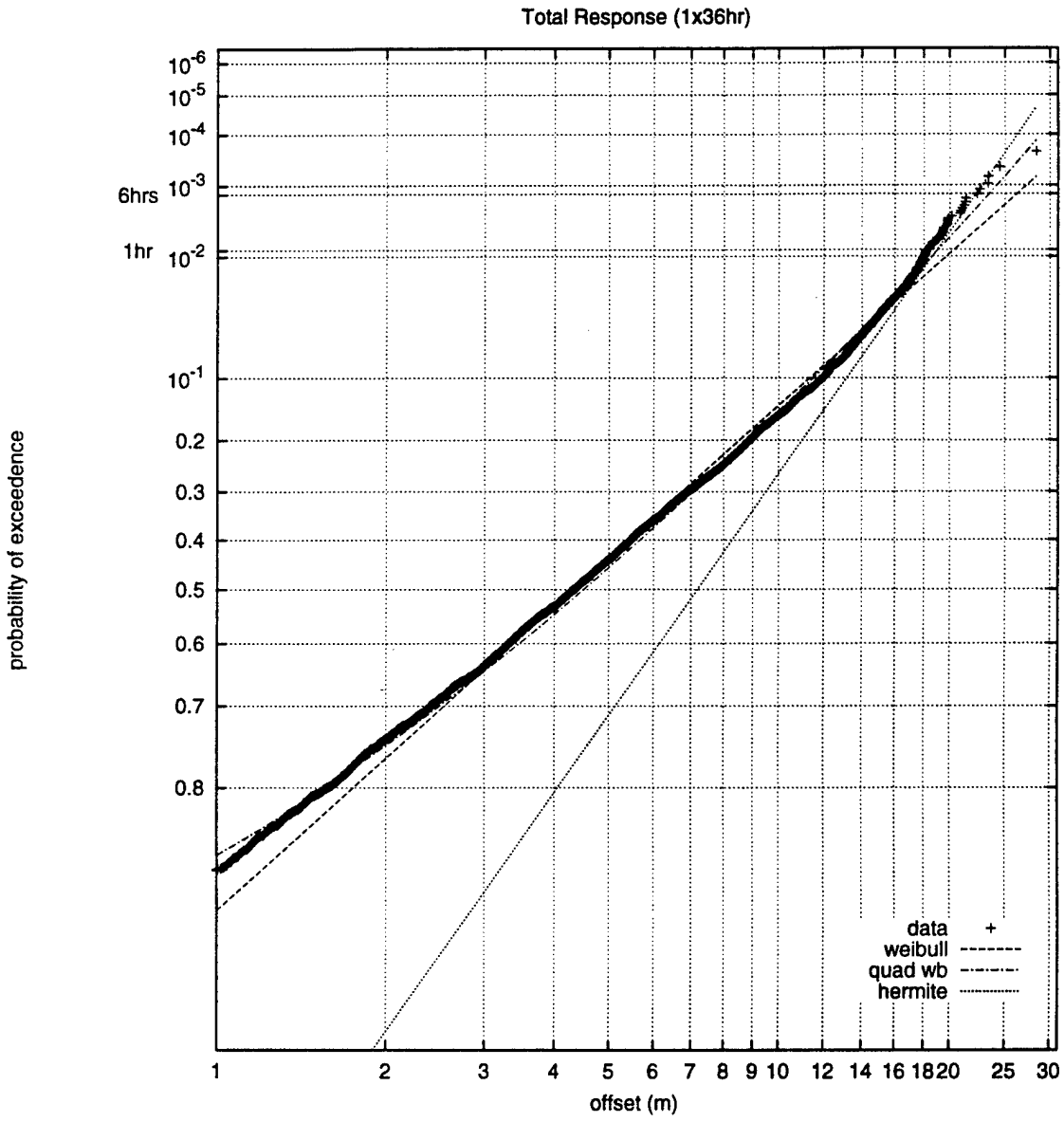

Figure 4.4: *Total response local peaks and fitted distributions plotted on Weibull-scale*

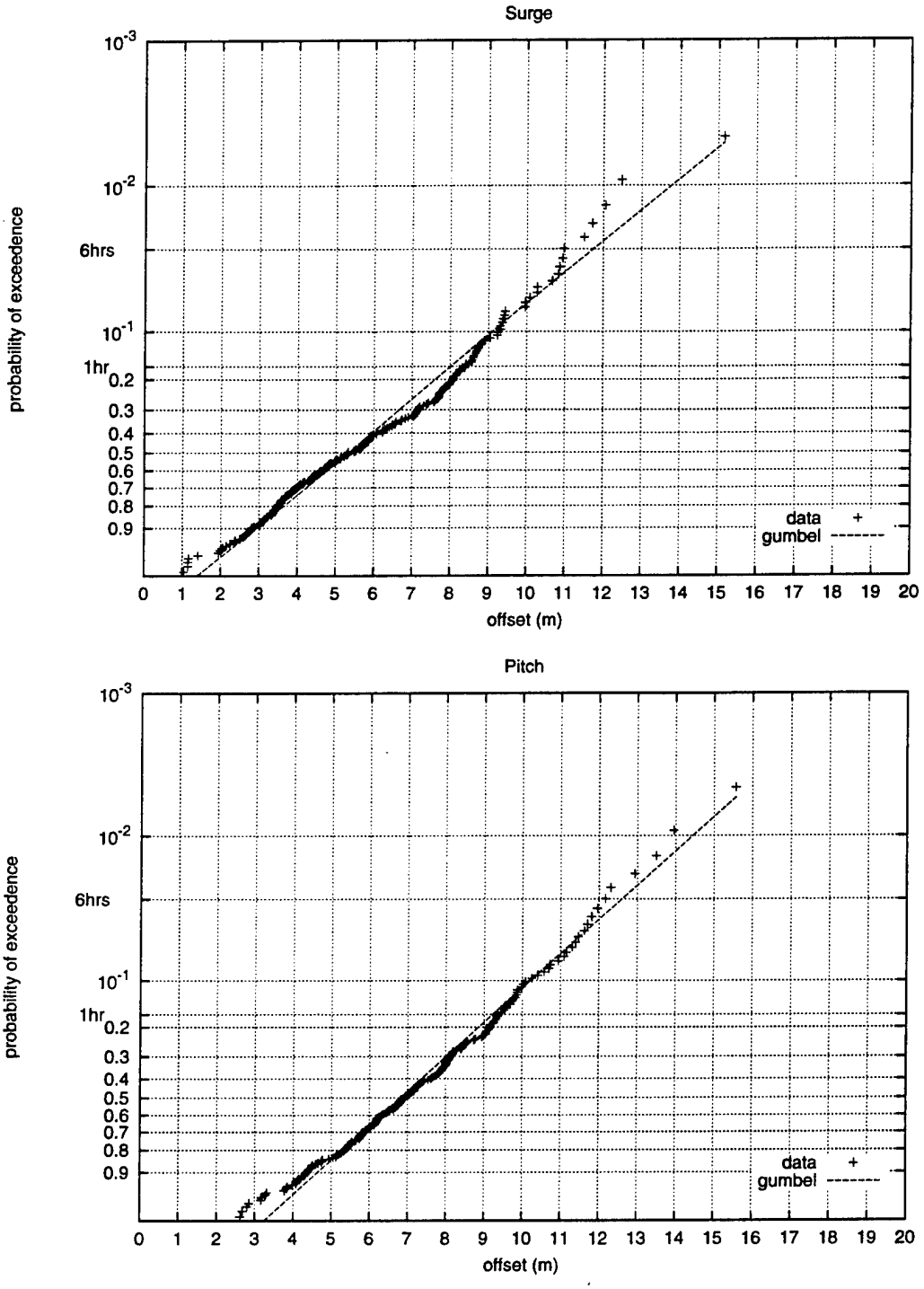

Figure 4.5: *Distribution of 10-minute global peaks plotted on Gumbel-scale (36 hours of data)*

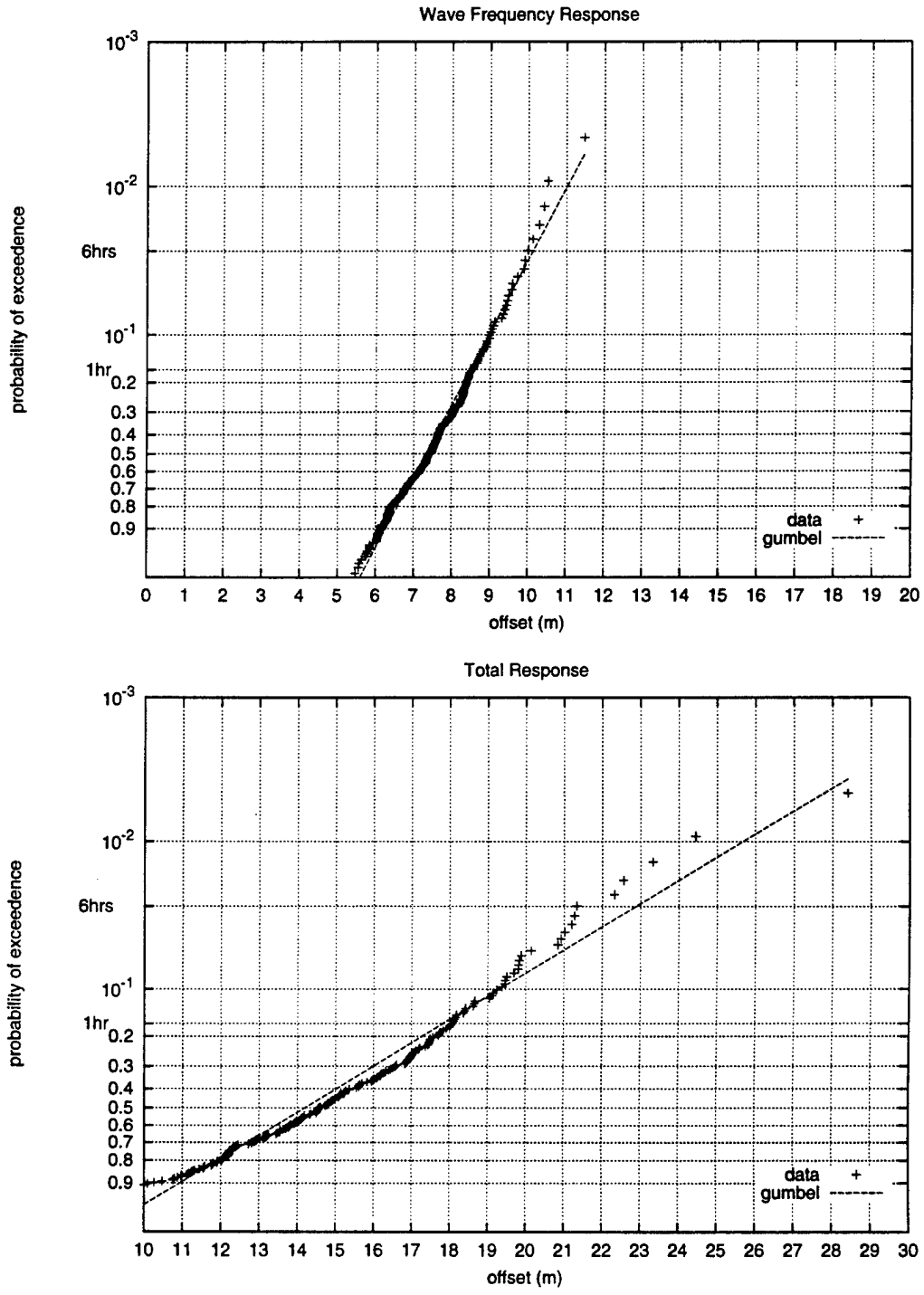

Figure 4.6: *Distribution of 10-minute global peaks plotted on Gumbel-scale (36 hours of data)*

The Extreme Value Distribution (1-hour global peaks)

Results in the preceding section treated the 36-hour simulation as one long data set, from which one can form "best" empirical distributions to compare with fitted models. In this section we return to considering the consequences of having only one hour of data (e.g. a single model test) to estimate statistics of X_{max}. We now treat the simulations as 36 1-hour segments, from which we can estimate both the bias and uncertainty that may arise in a single, randomly selected hour.

Surge

	Mean max	Obs_Stdv	CoV
Observed	8.76	2.21	0.252
Gumbel	8.78	2.18	0.248
Weibull	8.86	2.18	0.246
Q Weibull	8.69	2.13	0.245
Hermite	8.32	2.01	0.242

Wave frequency response

	Mean max	Obs_Stdv	CoV
Observed	8.96	0.94	0.105
Gumbel	8.98	0.87	0.097
Weibull	9.18	0.49	0.053
Q Weibull	8.91	0.62	0.070
Hermite	8.99	0.75	0.083

Pitch

	Mean max	Obs_Stdv	CoV
Observed	9.83	1.81	0.184
Gumbel	10.07	1.91	0.190
Weibull	10.76	2.04	0.190
Q Weibull	10.29	2.06	0.200
Hermite	10.01	2.04	0.204

Total

	Mean max	Obs_Stdv	CoV
Observed	19.12	2.66	0.139
Gumbel	19.08	2.24	0.117
Weibull	22.08	3.03	0.137
Q Weibull	19.99	2.45	0.123
Hermite	18.96	2.44	0.129

Table 4.3 *Predictions of 1-hour extremes, and their standard deviation based on 36 simulated hours, no bootstrapping*

Bias

We focus in table 4.3 on estimating μ_{Xmax}, the mean value of the hourly maximum. The "observed" mean max results are simply averages of the 36 simulated hourly max values. Compared with these unbiased observed estimates, the various models show rather consistent estimates of μ_{Xmax}. Biases are typically less than 5% (table 4.4); the only case of significant bias (15%) occurs when applying the Weibull model to the total set of

response peaks. This is entirely consistent with the results of the previous section. Note also that unlike the previous section, these results rely on the assumption of independent peaks when estimating $F_{Xmax}(x)$ (see eq.1.6) and hence μ_{Xmax}. The agreement found here suggests the adequacy of this assumption for extreme value estimation.

	Surge	Pitch	Wave freq.	Total
Gumbel	1.00	1.02	1.00	1.00
Weibull	1.01	1.09	1.02	1.15
Q Weibull	0.99	1.05	0.99	1.05
Hermite	0.95	1.02	1.00	0.99

Table 4.4 *Bias: the ratio between estimated and observed mean hourly extreme.*

Bootstrap Bias

The following table shows the ratio between the "observed" standard deviation and the average of the 36 bootstrap standard deviations. In order to calculate the latter, peaks of each simulated hour were resampled 200 times in the same fashion in chapter 3, to predict as many mean 1-hour extremes. From these 200 predictions the "bootstrap" standard deviation is calculated. Each of the 36 simulated hours was treated in this way to estimate the standard deviation; the bootstrap result reported here is the average of these 36 values. If bootstrapping provides an unbiased estimate of the standard deviation, this ratio should be equal to 1.Table 4.5 however shows this ratio is 2.1 on average, which clearly suggests that bootstrapping may underestimate the standard deviation.

	Surge	Pitch	Wave freq.	Total
Observed	2.46	4.02	1.92	1.94
Gumbel	1.86	1.95	1.55	1.35
Weibull	1.93	2.83	1.23	1.79
Q Weibull	2.05	3.43	1.32	1.68

Table 4.5 Ratio between the "observed" and bootstrap-estimated standard deviation
Note that for the Hermite no bootstrapping could be performed as it is fitted to the process, while we can only resample peaks.

Table 4.5 indicates that the bootstrap estimate of the standard deviation is much less biased for the wave frequency response predictions made with both Weibull models. The relatively large number of wave frequency peaks includes data far in the upper tail, which reduces the effect of the truncation of the distribution from which synthetic data sets are sampled. This truncation effect, which we believe may bias our estimate of the standard deviation, is much more severe for surge and pitch as they have less peaks. Surge and pitch peaks will also show higher correlation between peaks, an effect which bootstrapping analysis ignores.

Uncertainty

The wave frequency response also shows some reduction of the standard deviation of our prediction using a model (table 4.6). This effect is not observed for pitch and surge. Again we expect this reduction to be the result of the relatively large number of peaks in our data set, which reduces uncertainty in our estimate of the distribution parameters.

	Surge	Pitch	Wave freq.	Total
Gumbel	0.99	1.06	0.93	0.84
Weibull	0.99	1.13	0.52	1.14
Q Weibull	0.96	1.14	0.66	0.92
Hermite	0.91	1.13	0.80	0.92

Table 4.6 *Ratio between the "observed" and the from a model predicted standard deviation of the 1-hour mean extreme response*

An interesting observation is also that coefficient of variation of the peaks of the second order components, surge and pitch, is approximately twice as large as the coefficient of variation of the peaks of the first order component, the wave frequency response. This is

an effect that is generally observed for first and second order processes (e.g. Torhaug 1996).

SRSS

As it appears from the previous paragraph that the distribution of the total response is difficult to model, one might wonder whether the mean extreme total value can be estimated from its components, for which fairly straightforward models, such as a Rayleigh distribution, seem to suffice. The standard method that is used in random vibrations for this is the "square root of the sum of squares method", or srss. Although the method does not have a strong analytical background, it often gives good results for uncorrelated Gaussian processes. Extremes of a Gaussian process tend to be proportional to the standard deviation of the process. The standard deviation of the non-Gaussian total is equal to the "square root of the sum of squares" of the standard deviations of the Gaussian (Rayleigh) components, (plus the correlation terms which may become important for closely spaced modes). The prediction of the mean total 1-hour extreme response using the srss method for the observed values is $\sqrt{(8.76^2 + 8.96^2 + 9.83^2)} =$ 15.93 m. The observed value is 19.12 m. This relatively large difference may be due to either the correlation among these components, or to their non-Gaussian behavior (Naess and Røyset 1998). The srss method does not seem very useful in this particular case.

Improving Use of Limited Data

In the previous sections we concluded that fitting a model does not always reduce the uncertainty in our predictions of the mean (and distribution) of the hourly extreme value. All of our analysis however has been concentrated on predictions for, and based on, a 1-hour time period. Previous work by Torhaug (1996) shows that uncertainty can be reduced by a factor of roughly 2.5 for a jack-up structure, by fitting a model. In order to make a comparison between the statistics of the extreme response of a spar buoy and a jack-up structure, we will mimic the results found by Torhaug in this section. The most important difference is that the jack-up results were based on using 1-hour response histories to predict 6-hour mean extreme responses. The following table shows the results for the 6 observed 6-hour extremes, and the 36 predicted mean 6-hour extremes, based on 1 hour.

Surge

	Mean max	Obs_Stdv	CoV
Observed	11.76	1.71	0.15
Gumbel	11.76	2.96	0.25
Weibull	11.21	2.74	0.24
Q Weibull	10.77	2.59	0.24
Hermite	10.02	2.34	0.23

Wave frequency response

	Mean max	Obs_Stdv	CoV
Observed	10.35	0.62	0.06
Gumbel	10.45	1.39	0.13
Weibull	10.47	0.63	0.06
Q Weibull	10.06	0.84	0.08
Hermite	10.22	1.09	0.11

Pitch

	Mean max	Obs_Stdv	CoV
Observed	12.66	1.74	0.14
Gumbel	12.92	2.84	0.22
Weibull	12.61	2.47	0.20
Q Weibull	11.83	2.65	0.22
Hermite	11.46	2.64	0.23

Total

	Mean max	Obs_Stdv	CoV
Observed	23.31	2.67	0.11
Gumbel	23.34	3.57	0.15
Weibull	27.80	4.30	0.15
Q Weibull	24.07	3.39	0.14
Hermite	21.79	3.39	0.16

Table 4.7 *Predictions of 6-hour extremes, and their standard deviation based on 36 simulated hours, no bootstrapping*

Bias

The ratio between the best estimate of the mean 6-hour extreme value and the observed 6-hour extreme is reported in table 4.8. The differences between the predicted and observed values are often more pronounced because we are extrapolating a given model further into its tail. Now the Hermite predictions seem relatively low, while the Gumbel predictions appear to remain nearly unbiased. This may be because the Gumbel model is already fit to 10-minute maxes, hence requires the least extrapolation to reach the 6-hour level.

	Surge	Pitch	Wave fr.	Total
Gumbel	1.00	1.02	1.01	1.00
Weibull	0.95	1.00	1.01	1.19
Q Weibull	0.92	0.93	0.97	1.03
Hermite	0.85	0.91	0.99	0.93

Table 4.8 *Ratio of predicted extremes to observed 6-hour extreme*

Uncertainty

Table 4.7 shows the standard deviation increases if we estimate the mean 6-hour extreme not with the observed 6-hour extreme, but rather with a model fit prediction that only uses 1 hour of data. This effect is not surprising: results based on 1 hour of data should be more variable than those based on 6 hours. What is interesting however is that the increase in standard deviation of a single prediction of the 6-hour extreme is only roughly a factor of 1.5 on average.

What is reported in the first column of table 4.7 is the mean of 36 of these estimates for the fitted models, and the mean of 6 observed 6-hour extremes. The standard deviation of these estimated means, due to having a limited sample of 36 hours total, is the standard deviation reported in table 4.7 divided by the square root of the number of estimates. As the number of estimates is 6 for the observed extremes and 36 for the predicted extremes, the ratio between the observed and fitted standard deviations decreases by the square root of 6. The standard deviation of our best estimate of the 6-hour extreme therefore decreases by a factor $\sqrt{6}/1.5 = 1.6$ on average, suggesting extrapolating does help, although it is not as high as the 2.5 observed by Torhaug. Apparently the increase of uncertainty by extrapolating is less than the reduction caused by using more data.
The reductions of the coefficient of variation are reported below.

	Surge	Pitch	Wave fr.	Total
Gumbel	0.71	0.65	0.91	0.55
Weibull	0.69	0.58	0.41	0.55
Q Weibull	0.68	0.67	0.57	0.50
Hermite	0.66	0.68	0.73	0.55

Table 4.9 Ratio of the model-predicted *CoV of the mean 6-hour extremes to the CoV of the 6 observed extremes*

Bootstrap Bias

The following table confirms the bias of the bootstrap estimate of the standard deviation again, which is higher as we are extrapolating further out into the tails of the underlying distributions. Moreover the truncation of the distribution of peaks now also affects the predictions for the wave frequency response.

	Surge	Pitch	Wave fr.	Total
Observed	2.04	3.11	1.29	1.76
Gumbel	1.64	1.82	1.60	1.35
Weibull	1.62	2.55	1.26	1.81
Q Weibull	1.82	3.35	1.31	1.70

Table 4.10 *Ratio of observed CoV to bootstrap-predicted CoV of 6-hour extremes*

Extrapolation

The previous results for extrapolating leave us with the question of how small should we make the time periods to which we fit a distribution of extremes in order to predict an extreme value with the least amount of uncertainty. The smaller the period, the more we leverage the effect of having more estimates. On the other hand the shorter the periods, the further we need to extrapolate. The following tables report the bias and the reduction of the coefficient of variation compared to 1 hour for fitting the models to 20-minute periods, producing 108 estimates of the mean hourly and 6-hour extreme.

	Surge	Pitch	Wave fr.	Total
Gumbel	0.95	1.00	1.00	0.99
Weibull	0.94	1.00	1.02	1.14
Q Weibull	0.93	0.96	0.99	1.02
Hermite	0.84	0.92	0.99	0.93

Table 4.11 *Bias in 1-hour mean max predictions, based on 20 mins*

	Surge	Pitch	Wave fr.	Total
Gumbel	0.92	0.98	1.02	0.99
Weibull	0.88	0.89	1.01	1.18
Q Weibull	0.84	0.85	0.96	1.01
Hermite	0.72	0.80	0.97	0.86

Table 4.12 *Bias in 6-hour mean max predictions, based on 20 mins*

Not surprisingly relatively small biases become fairly large when we extrapolate further out in the tail. As the limited amount of data to which the models are fit can bias the higher moments relatively low, these higher-moment models may tend to underpredict extreme responses.

The effect of this extrapolation on the uncertainty in our estimates is shown in tables 4.13 and 4.14. These report the ratio of the coefficient of variation of the 108 1-hour and 6-hour predictions of the mean max based on 20 minutes, to the mean "observed" standard deviations for 1- and 6-hour periods (symbolically: $\sigma_{est}/\sigma_{direct}$, for 1 and 6 hour mean extremes). Table 4.13 is directly comparable to table 4.6.

	Surge	Pitch	Wave fr.	Total
Gumbel	0.81	0.81	0.79	0.77
Weibull	0.82	0.83	0.52	0.81
Q Weibull	0.80	0.80	0.62	0.72
Hermite	0.80	0.80	0.72	0.77

Table 4.13 *CoV reduction of 1-hour mean max based on 20 mins vs. 1hr*

	Surge	Pitch	Wave fr.	Total
Gumbel	0.13	0.19	0.15	0.12
Weibull	0.13	0.17	0.09	0.14
Q Weibull	0.16	0.24	0.13	0.14
Hermite	0.15	0.27	0.13	0.14

Table 4.14 *CoV reduction of 6-hour mean max based on 20 mins vs. 6hrs*

Without adding much extra bias, the variability in our estimate of the mean reduces despite extrapolating from a small amount of data for surge in particular (< 4 values on average). The average CoV reduction for the components is 0.76 (a factor of 1.3). We cannot reduce the time segment length any further for surge in view of its natural period of 5 minutes, as we need at least 3 peaks per period to fit the models. A similar argument has to be made for the Gumbel distribution, which needs at least 2 global periods within the time segment that will be fitted (20 mins). In a global period of 10 mins there will be 2 peaks in surge on average, for which a local peak model would probably be more appropriate. A global period less than 5 minutes would be meaningless for surge. Based on the previous considerations the segment length of 20 minutes was regarded as an absolute minimum for surge in this case. For the other components the data are not as scarce. The following tables show the result of extrapolating 6-minute periods to 1-hour extremes, and can be compared directly to tables 4.11 and 4.13.

	Surge	Pitch	Wave fr.	Total
Gumbel	-	0.97	1.09	1.22
Weibull	-	0.85	1.01	1.15
Q Weibull	-	0.66	0.78	0.71
Hermite	-	0.77	0.94	0.82

Table 4.15 *Bias in 1-hour mean max predictions, based on 6 mins*

	Surge	Pitch	Wave fr.	Total
Gumbel	-	0.62	0.69	0.75
Weibull	-	0.64	0.50	0.66
Q Weibull	-	0.62	0.51	0.54
Hermite	-	0.63	0.63	0.54

Table 4.16 *CoV reduction of 1-hour mean max based on 6 mins vs. 1hr*

As expected the data are insufficient for 1-hour extreme predictions in surge. However, also for pitch and the total and to a lesser extent for the wave frequency response, the results are very biased compared to the previous results. There still is a reduction of the CoV of our predictions, but this irrelevant with the amount of bias observed. Fitting to 6-minute periods and extrapolating to 10-fold periods of 1 hour clearly shows that using periods that are too short gives very poor results.

Conclusions

The results suggest that it is possible to reduce the uncertainty in our estimates of the mean extreme response, from limited data, by producing as many estimates of the mean extreme response as possible by fitting a model to short time segments. The limiting factors for the duration of these time segments is the minimum amount of data required to estimate the moments to fit to, and the amount of bias introduced in our predictions by using less data.

The results also suggest that the moments for the single hour of model test data are biased due to limited data, when they are compared to data from 36 hours of computer simulation. The local peaks of the components of the 36 hours of data showed very good agreement with a Rayleigh model. The local peaks of the total response, which is the sum of the three components, seems to be better described by a Hermite or quadratic Weibull model. The Gumbel model of the 10-minute global peaks showed good agreement for the total and all components.

1 CONCLUSIONS

In this report we have discussed estimation methods of the statistics of the extreme response of a spar buoy, during a 100-year Gulf of Mexico extreme sea state. We analyzed the statistics of a 1-hour time series of the horizontal offset at 54.8 m MWL, from a model test, and simulated 36 hours of response data using a computer model calibrated against the same model test. The statistics of interest were the mean of the distribution of the extreme response during a certain period of time, and the standard deviation of our estimate of that mean, quantifying the accuracy of our estimate. The results were compared and suggestions are made for more effective use of limited data.

The total spar buoy response consisted of 3 narrow-band processes with dominant frequencies at the structures natural periods in surge and pitch, and at the spectral peak period of the sea state. Predictions of the mean extreme hourly and 6-hourly response were made for the total response and all 3 components.

Predictions for a particular period of time were made fitting a parametric distribution to that period, using the 10-minute global peaks, all the local peaks, and the entire process, in order to investigate the effect of the amount of data included in the fit. The distributions were fitted to the moments of the selected data. The distribution models used were: (1) the Gumbel model (fitted to the 1^{st} 2 moments of the 10-minute global peaks), (2) the standard Weibull model (fitted to 1^{st} 2 moments of the local peaks), (3) a quadratic Weibull model (fitted to the 1^{st} 3 moments of the local peaks), and (4) a

Hermite transformation of the Rayleigh model (fitted to the 1st 4 moments of the process).

From the long duration simulated data (36 hours) we concluded that each of the 3 frequency components, the 2-parameter models capture their apparently Gaussian narrow-band behavior. For the observed short duration data (1 hour) the distributions of the components seemed considerably more narrow and "pinched". We believe this to be largely due to the effect of limited data, which biases the higher moments in particular. A similar bias was found from our 36 hours of simulation, if we processed it to estimate moments separately for each hour. Of course limitations of the computational model may also account partly for this discrepancy. The model used here was based on 2nd order diffraction analysis, including wave drift damping, viscous forces, and a constant mooring stiffness. The total response is wide-band mixture of 3 component processes, where peaks are not captured well by the standard Weibull models. This causes bias in our predictions of the statistics of the extreme response. The Hermite model, quadratic Weibull model, and the Gumbel model matched the total response better, and showed very little bias.

Estimates of the uncertainty in our predictions were made using non-parametric bootstrapping, and alternatively through simulation (or parametric bootstrapping). The results showed that bootstrapping local peaks, and negelecting their correlation, may not be very suitable to estimate statistics of extremes. As compared with the uncertainty found by long simulations, bootstrapping was found to underestimate the standard

deviation of our predictions of the mean 1-hour and 6-hour extremes. We therefore encourage the use of simulation – as opposed to non-parametric bootstrapping – to consider these issues of bias and uncertainty. While the computational model may not be perfect, it serves as a useful basis to preserve the distribution and correlation structure of the data, based on the best physical information at hand.

Based on the results of 36 hours of simulated response it appears that for all models the uncertainty in the predictions of the mean extreme value can be reduced by dividing the limited data in short-duration segments from which many estimates of the mean extreme response can be made by extrapolating a fitted model. It appeared that relatively very short segments reduced uncertainty most, without adding much bias.

APPENDIX A:

MOTIONS OF A SPAR BUOY IN RANDOM SEAS:

COMPARING PREDICTIONS AND MODEL TESTS

Alok K. Jha, P.R. de Jong, and Steven R. Winterstein

Presented at BOSS-97

To be presented at *BOSS-97*, Delft Univ., July 1997.

MOTIONS OF A SPAR BUOY IN RANDOM SEAS: COMPARING PREDICTIONS AND MODEL TEST RESULTS

Alok K. Jha, P. R. de Jong, and Steven R. Winterstein

Civil Engineering Dept., Stanford University

ABSTRACT

This study compares the analytically predicted motions of a floating spar buoy platform with the results of wave tank experiments. Results studied include extreme conditions in both the Gulf of Mexico and the North Sea. Base-case predictions combine nonlinear diffraction loads and a linear, multi-degree-of-freedom model of the spar stiffness and damping characteristics. Refined models add the effect of wave-drift damping, and of viscous forces as well. Consistent choices of damping and wave input are considered in some detail. These successive model refinements are generally found to improve agreement with the model test results.

KEYWORDS

Nonlinear wave diffraction; offshore structures; random vibration; spar buoys, structural reliability; wave tank experiments.

INTRODUCTION

This study describes ongoing research into the statistical response behavior and reliability of a particular deep-water floating structure: a spar buoy. Typically, the spar buoy concept involves a deep-draft, large-diameter cylindrical floating structure, with slack or taut mooring (e.g., Glanville et al, 1991). This concept has recently gained increased interest within the offshore community. For example, Oryx has installed the first production spar (Neptune) in 1996, while Chevron is currently designing the first spar (Genesis) for both drilling and production. Concurrently, a particular spar buoy has been designated the "theme structure" of the NSF-sponsored Offshore Technology Research Center (OTRC), centered at Texas A&M University and at the University of Texas at Austin.

This study compares analytical predictions of spar surge motions with the results of model tests from the OTRC wave tank (OTRC, 1995). Comparisons are shown both for summary response statistics and for complete time histories. Consistent choices of damping and wave input are considered in some detail. Responses are filtered and compared for three distinct frequency ranges: a relatively high-frequency contribution due to first-order wave energy, a low-frequency contribution due to

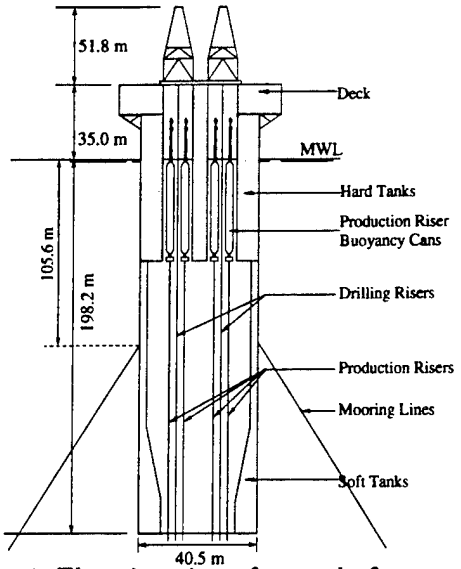

Figure 1: Elevation view of spar platform.

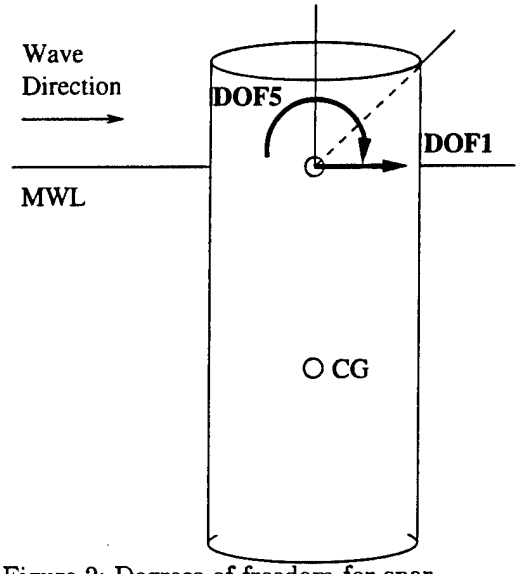

Figure 2: Degrees of freedom for spar.

pitch, and a still lower frequency contribution due to surge. Model tests are studied for extreme (100-year) conditions in both the Gulf of Mexico and the North Sea.

Results from analytical models are shown here over a range of increasing modelling detail. The base case includes nonlinear diffraction forces and a linear, multi-degree-of-freedom structural model. Refinements on this include the addition of wave drift damping, and then of viscous forces as well. These successively more detailed models are generally found to yield improved agreement with model test results. The analytical predictions also show the ability to capture another notable feature of the spar model tests; namely, the apparent "mode-swapping," between the spar response in pitch and surge modes, during the hour-long tests.

Spar Buoy Characteristics

Figure 1 shows the prototype dimensions of the spar buoy under study. Note its relatively deep draft (H=198.2m), particularly with respect to its diameter (D=40.5m). For prediction purposes the spar buoy hull is assumed rigid, and its mooring lines are modelled as a set of massless, linear springs. To predict the spar's motions in the along-wave direction, we adopt a 2DOF model that includes the surge motion $x_1(t)$ and pitch rotation $x_5(t)$ at the mean water level* (Figure 2). At an elevation z above this level, the corresponding along-wave displacement of the rigid spar is predicted simply as $x_1(t) + z \cdot x_5(t)$. In particular, we apply this result here with z=54.8m, to compare with video-recorded surge motions at this elevation during the wave tests (OTRC, 1995).

Mode Shapes and Periods

Assuming small deformations, the 2×2 stiffness and mass matrices can be constructed from geometrical considerations (Jha, 1997). This mass matrix includes added mass terms, reflecting first-order

*Note that we retain the common convention that numbers surge and pitch DOFs as "1" and "5" respectively, although no other DOFs are included here.

wave radiation effects. The resulting mode shapes and natural frequencies are

$$f_1 = \frac{1}{330}\ [\text{Hz}],\ \phi_1 = [1 \quad 0]^T; \qquad f_5 = \frac{1}{70}\ [\text{Hz}],\ \phi_5 = [100 \quad 1]^T \tag{1}$$

These modal frequencies agree well with the natural periods, T_1=330s and T_5=67s, estimated from free-decay tests of the spar (OTRC, 1995). Note that this lower-frequency mode involves a pure translation, while the higher-frequency mode reflects a pure rotation about an axis located at depth 100m below the MWL. (Equivalently, Eq. 1 implies that a small rotation x_5 [rad] is accompanied by a translation of x_1=100x_5 [m] at the MWL.) These modes directly reflect the translational and rotational stiffnesses, respectively, of the spar's mooring system.

Qualitative Results and Consistent Damping Estimates

We consider here the spar model tests that reflect extreme, roughly 100-year wave conditions. We also focus on tests that apply wave loads only, neglecting other tests that include simultaneous current and/or wind loads. This leaves us with three model tests, each lasting 1 hour (all time and length units here reflect prototype scale). Two of the three are separate realizations of 100-year Gulf of Mexico seastates, while the third models 100-year North Sea conditions. We refer here to these seastates as "GOM1", "GOM2", and "NS". (In OTRC internal reporting, these tests are respectively denoted "aran3", "aran4", and "aran5". To date, only "aran3" has received systematic study by OTRC investigators; e.g., Ran et al, 1996, Weggel and Roesset, 1996).

Wave Measurements and Characteristics

A reference, "undisturbed" wave elevation history has been measured during the OTRC tests by a probe located 125m (prototype scale) from the spar, in a direction perpendicular to the wave direction. The spectra of these waves are found to be relatively well-fit by JONSWAP spectral shapes with γ=2; the significant wave height and peak period values are estimated as H_s=14.1m and T_p=14.1s for the Gulf of Mexico seastates, and H_s=14.8m and T_p=16.1s for the North Sea test (Jha, 1997). Note however that our response predictions use the observed wave histories from the tests, and not the simulated input from a theoretical wave spectral model.

Response Measurements and Characteristics

Figure 3 shows the power spectrum of the spar displacement, measured at height z=54.8m above MWL, during the GOM1 test. Note its two low-frequency modes, at around f_1=1/330 and f_5=1/70 Hz, reflecting motions induced by surge and pitch resonance. As Figure 3 shows, we use bandpass filters here to separate the observed surge component (0–.006 Hz), pitch component (.006–.03 Hz), and remaining wave frequency component (above .03 Hz). This gives rms response contributions of σ_{surge}=3.4m, σ_{pitch}=4.0m, and σ_{wave}=2.5m. Thus a linear force model, which predicts energy only at the wave frequencies, would capture only a small portion of the response rms. It would also completely fail to predict the mean response, here found to be 4.9m. The other tests offer similar results. This shows the need for models of nonlinear forces—diffraction, drag or both—to explain not only the mean offset but also the amplitude of slow-drift oscillations for the spar. The effects of both nonlinear diffraction and drag loads are considered below.

Figure 4 shows the corresponding time history of the response during the GOM1 test. Both the total response and its filtered components are shown. Consistent with its power spectrum in Figure 3, the response indeed displays three distinct time scales. What Figure 3 fails to reveal, however, is that the relative contribution of the different frequency components does not remain constant over time. For the GOM1 test, the observed response changes qualitatively at around t=1500s, when

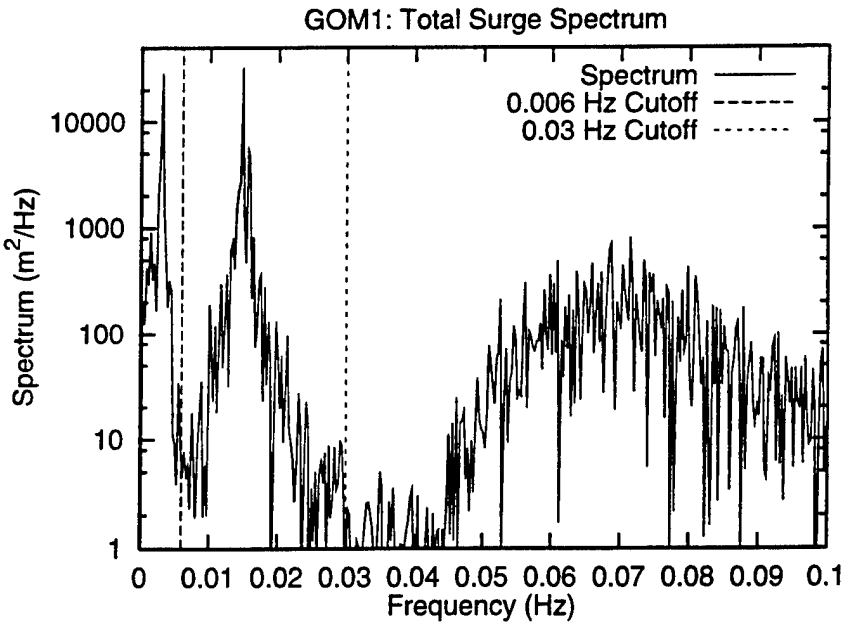

Figure 3: Spectrum of measured surge displacements at 54.8m elevation above MWL for GOM1 seastate

the surge component begins to contribute significantly. The other tests show somewhat similar shifts between the energy in surge and pitch modes—although this "mode swapping" is observed at different times, and for different durations, in different tests. The wave input histories show no such episodic nature. This reflects a further modelling challenge: can analytical models predict not only the correct average frequency content (e.g., the spectrum in Figure 3), but also time-domain behavior consistent with Figure 4? Clearly, this time-domain evolution of surge and pitch components depends directly on (1) their initial conditions at the beginning of the test recording and (2) the damping values assigned to these modes. We therefore discuss these issues, particularly damping estimation, in some detail.

Estimating Initial Conditions

In the experiments, spar motions were recorded after about 15 minutes (prototype scale), when the wave tank conditions were deemed to have achieved steady-state conditions. Thus, the assumption of at-rest initial conditions would corrupt our predictions, more so in the surge mode which contains relatively few cycles over the hour-long test. To avoid this, our predictions use initial conditions consistent with the tests; i.e., for each test we filter the observed motions to estimate surge and pitch components (e.g., Figure 4). The initial values/velocities of these components are then used to start our slow-drift motion predictions (Jha, 1997).

Estimating Surge and Pitch Damping

Because the tests include relatively few cycles of lightly damped motion, it is challenging to form precise damping estimates from them. We focus here on frequency-domain damping estimates, using response spectra from the various tests (e.g., Figure 3). One may, for example, select dampings

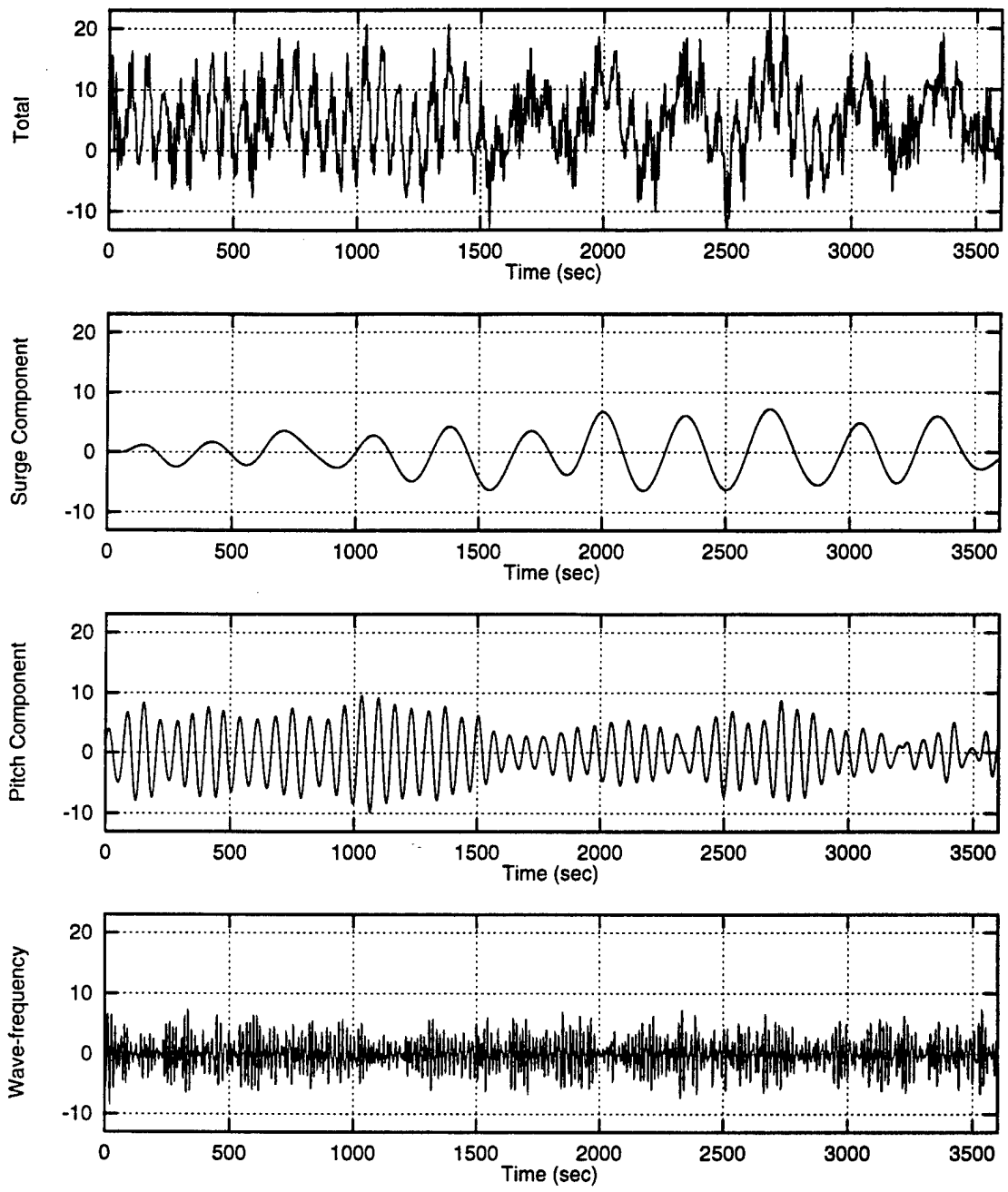

Figure 4: Total measured horizontal displacement and its filtered surge, pitch and wave-frequency components for GOM1 seastate

ζ_i so that our analytical model predicts the correct *area* under each of these observed spectral modes (i.e., the variances σ^2_{surge} and σ^2_{pitch}). A danger in this approach is that it may mask a force modelling error (e.g., Ude, 1994). For example, if predicted forces are overestimated we may overestimate damping in an effort to compensate. Thus, we instead seek damping values to preserve the observed spectral *shape*—the rms values σ_{surge} and σ_{pitch} are reserved to test the model's adequacy. One such measure of spectral shape is the half-power bandwidth, at which the response spectrum decays to half its peak value. By setting this bandwidth to its approximate value from theory—$f_{HP}=\pm\zeta_i f_i$ to either side of the natural frequency f_i—one can estimate the damping ζ_i from an observed power spectrum. For example, if the spar buoy has damping ζ_1=.05 at the surge frequency f_1=1/330, we find f_{HP}=1/6600 Hz. Unfortunately, from a T=1-hour history, our finest frequency resolution is $df=1/T$=1/3600 Hz—too coarse to resolve the half-power bandwidth, even if no frequency-averaging is applied to the observed spectrum.

We are therefore led to consider the average shape of the response spectrum across frequencies, as measured by the unitless bandwidth measure δ (Vanmarcke, 1972):

$$\delta = \sqrt{1 - \lambda_1^2/(\lambda_0\lambda_2)}\,; \quad \lambda_n = \int f^n S_x(f) df \tag{2}$$

Note that in general, any parameter of the form $\delta_n=[1 - \lambda_n^2/(\lambda_0\lambda_{2n})]^{1/2}$ could be used to reflect bandwidth: $\delta_n \to 0$ as the bandwidth narrows. Perhaps the most widely used is δ_2, e.g. in modelling peaks of a Gaussian process. We use δ with n=1 here, as its lower spectral moments are less sensitive to high-frequency spectral content. We apply Eq. 2 twice, over the frequency ranges of surge (0–.006 Hz) and pitch (.006–.03 Hz) components, to find separate δ values that characterize their respective modal bandwidths.

For a 1DOF system under broad-band loads, δ can be related directly to the damping level (Vanmarcke, 1972, Ude and Winterstein, 1996). To form estimates consistent with our 2DOF model, however, we select damping ratios ζ_1 and ζ_5 so that our predicted response shows the same δ values, in both the surge and pitch frequency ranges, as found from the observed responses. This is an iterative process, which must be performed for each choice of (1) seastate and (2) predictive response model. We differentiate here between 2 seastates (GOM1 and GOM2 versus NS), and among 4 predictive models. These models are described below, together with the 2 × 4 values of modal dampings that result. In each case, a corresponding damping matrix $\boldsymbol{C}$ is inferred from the mass matrix and the matrix $\boldsymbol{\Phi}$ of modal shapes: $\boldsymbol{C}=\boldsymbol{M\Phi Q\Phi}^{-1}$ in terms of $\boldsymbol{Q}$=diag$(4\pi\zeta_i f_i)$.

Predictive Models of Forces and Damping

Our first, base-case model applies diffraction forces only (the "**DF**" model). Linear diffraction gives first-order transfer functions $F_1^{(1)}(\omega_k)$ and $F_5^{(1)}(\omega_k)$, the (complex) amplitude of surge force and pitch moment due to a unit-amplitude wave at frequency ω_k. A corresponding second-order diffraction analysis gives $F_1^{(2)}(\omega_k,\omega_j)$ and $F_5^{(2)}(\omega_k,\omega_j)$, the surge and pitch excitation amplitudes at the difference frequency $\omega_k - \omega_j$ due to pairs of incident waves at frequencies ω_k and ω_j (Kim and Yue, 1989; Kim and Yue, 1991). These subharmonic excitations drive the surge and pitch resonant motions, which dominate the spar response (e.g., Figure 3). Note that these diffraction forces assume as input not the undisturbed total wave elevation/potential but rather its first-order component. Here we use new methods (Winterstein and Jha, 1997) to identify the underlying first-order contribution to the observed undisturbed wave.

For this model, the damping matrix $\boldsymbol{C}$ gives the major source of damping. For example, Table 1 shows that this DF model requires the damping ratios ζ_1=4.5% and ζ_5=1.6% to match the spectral bandwidths estimated from the 2 GOM tests. In this (and other cases) the single NS test suggests rather lighter damping; indeed, an effectively zero value of pitch damping is not always able to give

Model	Description	GOM		NS	
		ζ_1	ζ_5	ζ_1	ζ_5
DF	Base-case model with diffraction forces	4.5	1.6	1.7	.001
DF/WDD	DF model plus wave-drift damping	3.3	0.6	.001	.001
DF/WDD/VF(u)	DF/WDD model plus viscous forces from undisturbed waves	4.0	0.5	2.5	.001
DF/WDD/VF(d)	DF/WDD model plus viscous forces from disturbed waves	6.5	.001	0.1	.001

Table 1: Description of 4 models, and consistent damping ratios ζ_1 and ζ_5 in surge and pitch.

as narrow a spectral bandwidth as observed. Note, however, that the NS test includes only a single hour, making narrow bandwidths more difficult to estimate than over the combined, two hours of GOM tests.

Our second model (**DF/WDD**) includes both diffraction forces and wave-drift damping. This damping force is proportional both to the structural velocity and to the square of the wave amplitude. The resulting nonlinear damping will tend to offset large slow drift forces, and perhaps reduce the extreme peaks of the surge response. We may expect that once wave drift damping is added, we require lower values of the additional modal damping ζ_i than in the DF model. Table 1 shows that this is indeed the case.

Finally, we also implement two models that include viscous drag forces as well as diffraction effects. These differ only in their choice of wave input: one uses the undisturbed waves, while the other uses the disturbed waves near the spar, inferred from its reported heave motions and the air-gap (structure-to-wave distance) measurements. Both models use the Morison's drag term with C_D=0.6, and Wheeler stretching (Wheeler, 1970) to integrate effects from the spar bottom to the free surface. They also both use the absolute fluid velocity; relative velocity effects are assumed reflected through damping terms.

Numerical Results

Wave-Frequency Response

We first compare the wave-frequency portions of the predicted and observed spar responses. These observed portions are found by applying a high-pass filter, with a low-frequency cutoff of .03 Hz., to the measured displacement histories. Figure 5 shows that these predictions fairly accurately predict not only the qualitative response behavior, but also its detailed cycle-by-cycle evolution in all three tests. This suggests that our models accurately reflect first-order wave forces, and the mass properties of the spar. (Because slow-drift forces and damping do not affect this wave-frequency response, all four of our models predict roughly the same histories in Figure 5. Thus, for clarity Figure 5 shows predictions only for the simplest (DF) model.)

Slow Drift Response

Figure 6 compares the predicted and observed moments of the slow-drift response. Results are shown for the rms values σ_1 and σ_5, corresponding to frequency ranges (0–.006 Hz) and (.006–.03 Hz), and for the total mean offset (which cannot be split directly into surge and pitch contributions).

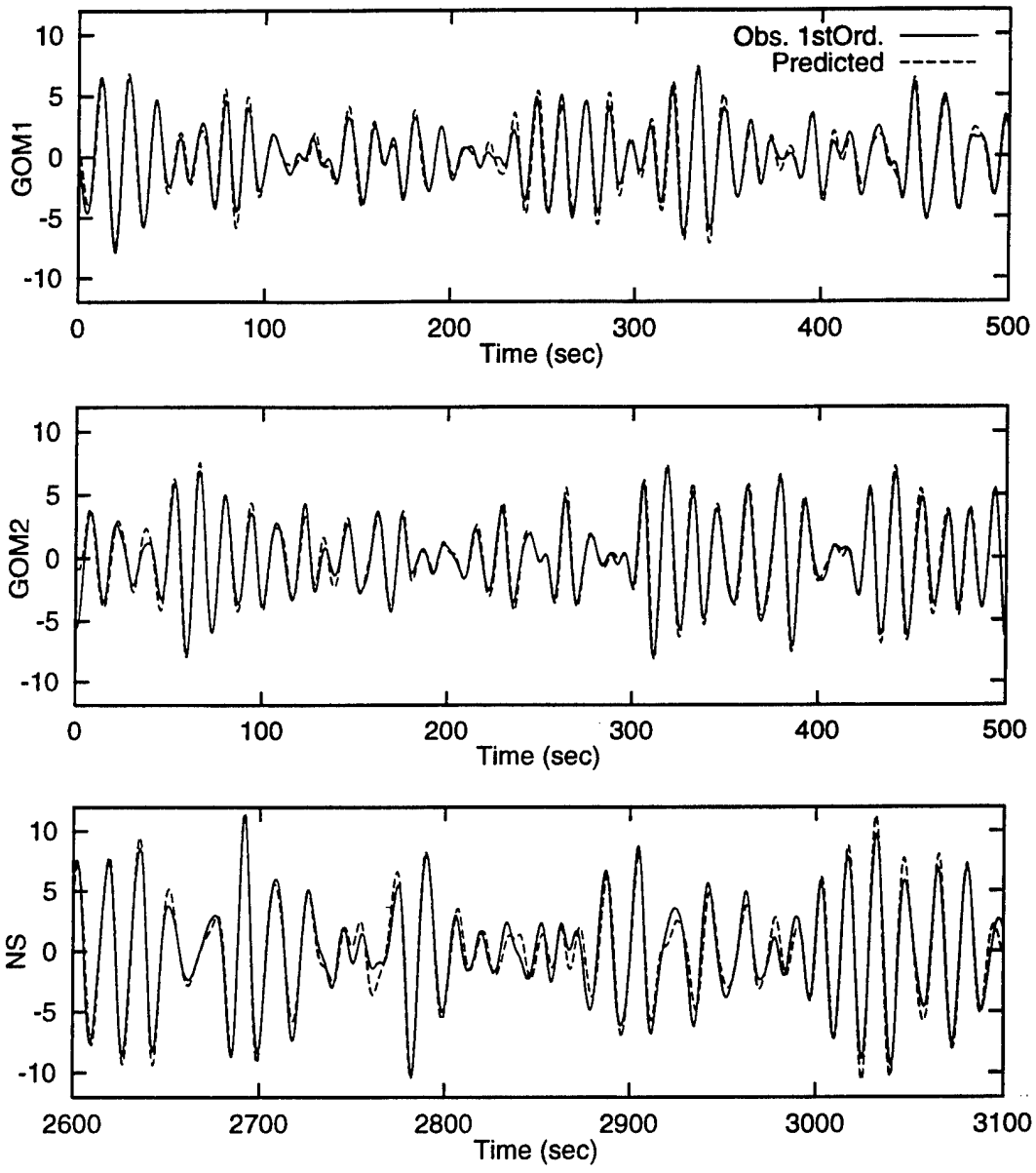

Figure 5: Predicted vs. observed first-order response histories for the three tests. For clarity we show only 500-second portions of each test, selected to include the absolute maximum observed response.

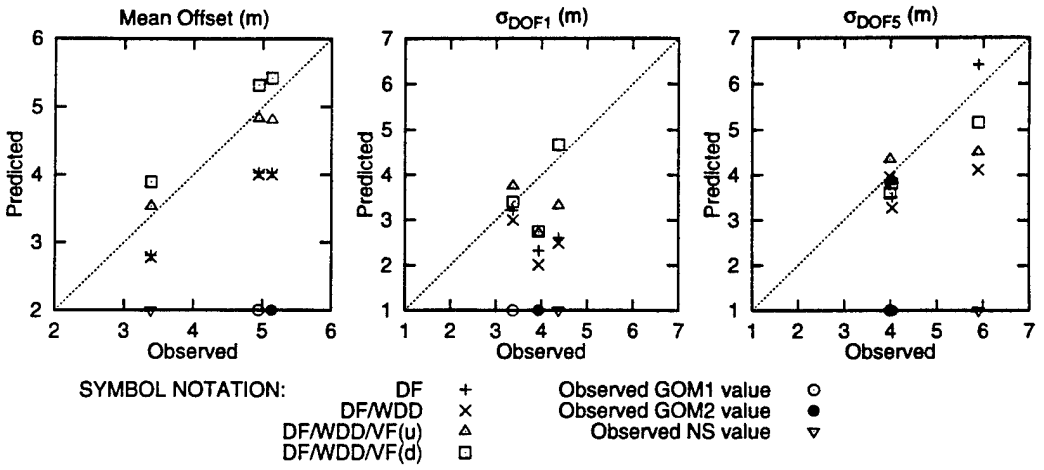

Figure 6: Predicted response mean and standard deviations vs measured results in the three tests. Standard deviations are shown for both surge and pitch frequency components.

In each case the predicted values from all 4 models are plotted against the observed value from that test. Because there are 3 tests, this results in 4 × 3=12 data points per plot. A 45-degree line implying perfect agreement is also shown.

Focusing first on the diffraction-only (DF) model, we find it underpredicts both the mean and rms in all but one of the 9 observed values. (We return below to the anomalous case, which involves the pitch rms σ_5 in the NS test.) Adding wave drift damping (DF/WDD) will not change the mean, and only weakly affects the rms predictions (again excluding the NS pitch case). This suggests the need for viscous forces, which contribute both an extra mean force (due to the asymmetric effect of wave stretching) and a slowly-varying drift force. As Figure 6 shows, the VF(u) and VF(d) models—which include viscous forces—generally give better predictions of both the mean and rms levels. Results with the disturbed wave (VF(d)) generally give slightly higher responses—both in mean and rms—than those using the undisturbed wave (VF(u)). Neither the VF(u) nor VF(d) model seems systematically closer to the observations; however, both appear superior to models that exclude viscous forces altogether.

Returning to the anamolous pitch response in the NS test, note from Table 1 that our damping calibration effectively fails in this case. Although each of the 4 models was assigned only minimal pitch damping (ζ_5=.001), all of these predict wider spectral bandwidths than that observed in the NS test. Thus the predictive models here are not "damping-tuned" to the tests as in the other cases—and the pattern of the 4 model predictions for σ_5 in the NS case is somewhat arbitrary. As to why the bandwidth mismatch may occur, recall the increased effect of limited data in the NS case: here the bandwidth estimation uses only the 1 hour test, as opposed to the 2 pooled hours used to form the predictive model for both GOM seastates.

Total Response Histories

Finally, we compare the observed and predicted 1-hour histories of the total spar displacement. Figures 7–9 show these histories for the 3 1-hour tests. All figures show the observed displacement history at the top, while 3 of the 4 corresponding predictions are shown beneath (the DF/WDD

model is omitted for clarity). Recall that our particular interest lies in predicting not only overall response statistics, but also the response evolution and potential mode-swapping (e.g., Figure 4 for the GOM1 case). Figure 7 repeats that case, and it is notable that all 3 predicted responses show a similar trend, toward greater surge response, in the second half of the GOM1 test. Note also that for extreme response events (e.g., observed response above 20m), all of the predictions show fairly good agreement. The greatest deviations, between the test and predictions, seem to occur over periods of relatively low response amplitude (e.g., times t=0–1000s, 1500–2300s).

Figure 8 shows similar tendencies for the GOM2 test. Again there is good qualitative agreement: both the tests and the predictions show a period of relatively little surge (at around t=700–2000s), followed by a marked surge increase through the rest of the hour. Large observed responses tend to coincide with high predicted values. The magnitude of these large responses is not as well predicted, however; predictions generally underestimate the response in the critical high-surge portion (t=2300–3600s). In contrast, the same predictions often overestimate response in the earlier, low-surge segment (t=700–2000s). (This potential for mode swapping and compensating errors suggests the need here to compare observations and predictions through time history behavior, not merely through summary statistics in the time or frequency domain.)

Finally, Figure 9 shows NS test results. Again there is a transition, near the end of the test, which produces the largest amplitude responses (indeed, the largest offsets among the 3 tests). It is caused here, however, by an increase in the pitch as well as the surge component. Note that despite the potential damping mismatch in this case, the models follow this critical portion of high-amplitude pitch fairly well (from about t=2700s on). As in the GOM1 case, greater deviations between models and observations occur at earlier portions of the history, involving lower amplitude responses.

Comparing Responses to Simulated and Observed Waves

The foregoing results show how well various models can predict the spar response in the OTRC tests, based on the corresponding observed wave input. Finally, we study briefly an associated question: are the observed response properties, such as mode swapping, also consistent with the response of the spar to idealized, Gaussian simulations of (first-order) random waves? If not, these observed properties may perhaps reflect special aspects of the wave input in the wave tank; e.g., the effect of its finite dimensions.

As earlier noted, both surge and pitch rms components of the observed spar motions vary notably over periods of roughly 20–30 minutes. We quantify this rms variation by (1) splitting the response into 20-minute segments; (2) calculating the rms values, $\sigma_1 ... \sigma_n$, in each of the n segments; and (3) forming the sample mean $\overline{\sigma}=\sum_i \sigma_i/n$ and variance $s_\sigma^2=\sum_i(\sigma_i-\overline{\sigma})^2/(n-1)$. We focus here on the two GOM tests, yielding 2 hours and hence n=6 20-minute segments with associated rms values $\sigma_1 ... \sigma_6$. The resulting s_σ values are found to be

$$s_\sigma = 1.22\text{m (surge)}; \quad s_\sigma = 0.50\text{m (pitch)} \tag{3}$$

For comparison we simulate† multiple 2-hour spar histories, and process each as we did the 2-hour test to find a corresponding s_σ estimate. These s_σ estimates from our simulations yield the following

†These simulations use the DF/WDD/VF(u) model, and first-order Gaussian waves are simulated from a JONSWAP spectrum with H_s=14m, T_p=14s, and γ=2. The diffraction analysis internally applies second-order corrections to the (assumed) first-order wave input; hence the Gaussian model is consistent here. Drag forces for this model use the total undisturbed wave; for simplicity we use the Gaussian waves here as well. Alternatively, one may add second-order wave contributions to better approximate the total undisturbed wave.

mean $E[s_\sigma]$ and standard deviation $D[s_\sigma]$:

$$E[s_\sigma] = 1.26\text{m (surge)}\,; \quad E[s_\sigma] = 0.95\text{m (pitch)} \tag{4}$$

$$D[s_\sigma] = 0.47\text{m (surge)}\,; \quad D[s_\sigma] = 0.45\text{m (pitch)} \tag{5}$$

Thus, while the observed modal rms values may seem highly variable, our simulations show similar or *still greater* variability (especially in pitch). Note also that the $D(.)$ values here reflect variability in s_σ estimates from different T=2 hour segments. (If T increases, $D(.)$ should decay like $T^{-1/2}$.) Because Eq. 3 uses 1 T=2 hour segment, these $D(.)$ values suggest the following mean $\pm$1-sigma intervals on the test estimates: s_σ=1.22 $\pm$ 0.47 in surge and s_σ=0.50 $\pm$ 0.45 in pitch. As even these relatively narrow, 1-sigma confidence intervals include the average simulation results (Eq. 4), it is difficult to find statistically significant differences between the tests and the simulations.

Conclusions

Four models have been established to predict the along-wave motions of a spar buoy in random seas. These have been implemented and compared with wave tank measurements of the spar displacement, at a reference elevation z=54.8m above the mean water level. Results are shown across 3 1-hour tests of 100-year extreme wave conditions. Specific methods and results include the following:

- In all of the tests, the main rms contribution comes from the resonant response in surge and pitch modes, at periods of roughly 330s and 70s respectively (e.g., Figure 3). This shows the need for models of nonlinear forces—diffraction, drag or both—to explain not only the mean offset but also the amplitude of slow-drift oscillations of the spar.

- The significant low-frequency resonant response also implies the need for accurate estimates of damping, in both the surge and pitch modes of the spar. We show how these modal dampings can be estimated from response spectral moments. The resulting dampings are "consistent" with the other features of the model; for example, the explicit addition of wave drift damping (WDD) is accompanied by lower levels of the remaining damping in the model (Table 1).

- The wave-frequency response has been found to be fairly well predicted across all 3 tests (Figure 5). This reflects the modelling adequacy of linear diffraction forces and the spar's mass properties. Regarding slow-drift response, models that include only diffraction forces generally underestimate both the mean and rms response levels (Figure 6). To address this, we introduce additional models that include viscous forces, based on either the undisturbed (far-field) wave or the actual disturbed wave in the presence of the spar. While it is difficult to conclude which of these is generally more accurate, both appear superior to models that exclude viscous forces altogether.

- The observed responses display considerable "mode-swapping" between surge and pitch modes (e.g., Figure 4). Figures 7–9 show that our predictive models, which use the observed wave and its underlying first-order components, can produce qualitatively similar behavior. They generally follow the observed trend, in all three tests, toward larger amplitude responses near the end of the hour. This trend manifests itself in the Gulf of Mexico tests by a late increase in surge-induced response (Figures 7–8), and in the North Sea test by enhanced pitch response as well (Figure 9).

- While the modal rms values in the tests appear rather variable, long simulations with Gaussian (first-order) waves show similar or *still greater* variability (Eqs. 3–5). From the limited 2-hour duration of GOM tests, it is difficult to find statistically significant differences between these tests and the simulations.

Acknowledgements

Support for this work has been provided by the National Science Foundation, through a grant from its Offshore Technology Research Center. We gratefully acknowledge the OTRC for their ongoing technical and financial support.

REFERENCES

Glanville, R.S., J.R. Pauling, J.E. Halkyard, and T.J. Lehtinen (1991). Analysis of the spar floating drilling production and storage. *Proc., Offshore Tech. Conf.,* Houston, Paper OTC–6701, 57–68.

Jha, A.K. (1997). *Nonlinear stochastic models for ocean wave loads and responses of offshore structures and vessels,* Ph.D. thesis, Civil Eng. Dept., Stanford University.

Kim, M.H. and D.K.P. Yue (1989). The complete second-order diffraction solution for an axisymmetric body. Part 1: Monochromatic incident waves. *Journal of Fluid Mech.,* **200**, 235–264.

Kim, M.H. and D.K.P. Yue (1991). Sum- and difference-frequency wave loads on a body in unidirectional Gaussian seas. *J. Ship Res.*, **35**, 127–140.

OTRC, Vol. I. (1995). *Spar model test: joint industry project,* Final Report, Offshore Technology Research Center.

Ran, Z., M.H. Kim, J.M. Niedzwecki, and R.P. Johnson (1996). Responses of a spar platform in random waves and currents (experiment vs. theory). *Int. Journal of Offshore and Polar Eng.,* **6**(1), 27–34.

Ude, T.C. (1994). *Second-order load and response models for floating structures: probabilistic analysis and system identification,* Ph.D. thesis, Civil Eng. Dept., Stanford University.

Ude, T.C. and S.R. Winterstein (1996). Calibration of slow-drift motions using statistical moments of observed data. *Proc., 6th Int. Conf. Offshore & Polar Eng.,* Los Angeles.

Vanmarcke, E. (1972). Properties of spectral moments with applications to random vibration. *J. Engrg. Mech.,* ASCE, **98**, .

Weggel, D.C. and J.M. Roesset (1996). Second-order dynamic response of a large spar platform: numerical predictions versus experimental results. *Proc., 15th Int. Conf. Offshore Mech. & Arctic Eng.,* Florence.

Wheeler, J.D. (1970). Method for calculating forces produced by irregular waves. *Journal of Petroleum Tech.,*, 359–367.

Winterstein, S.R. and A.K. Jha (1997). Random nonlinear ocean waves: a method to identify first- and second-order effects. *J. Engrg. Mech.,* ASCE, Submitted for possible publication.

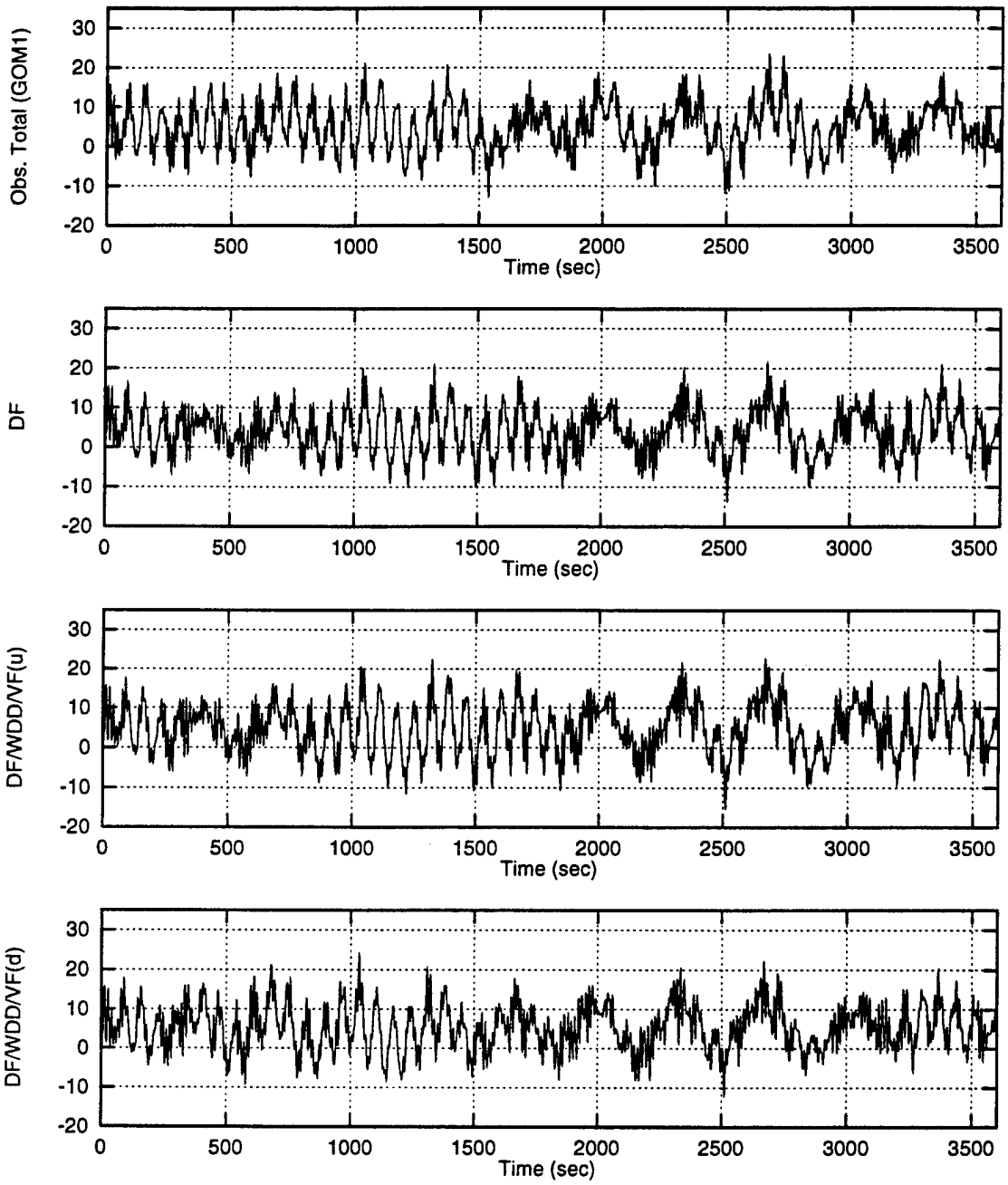

Figure 7: Combined (total) surge response time history for GOM1: prediction vs. measurement.

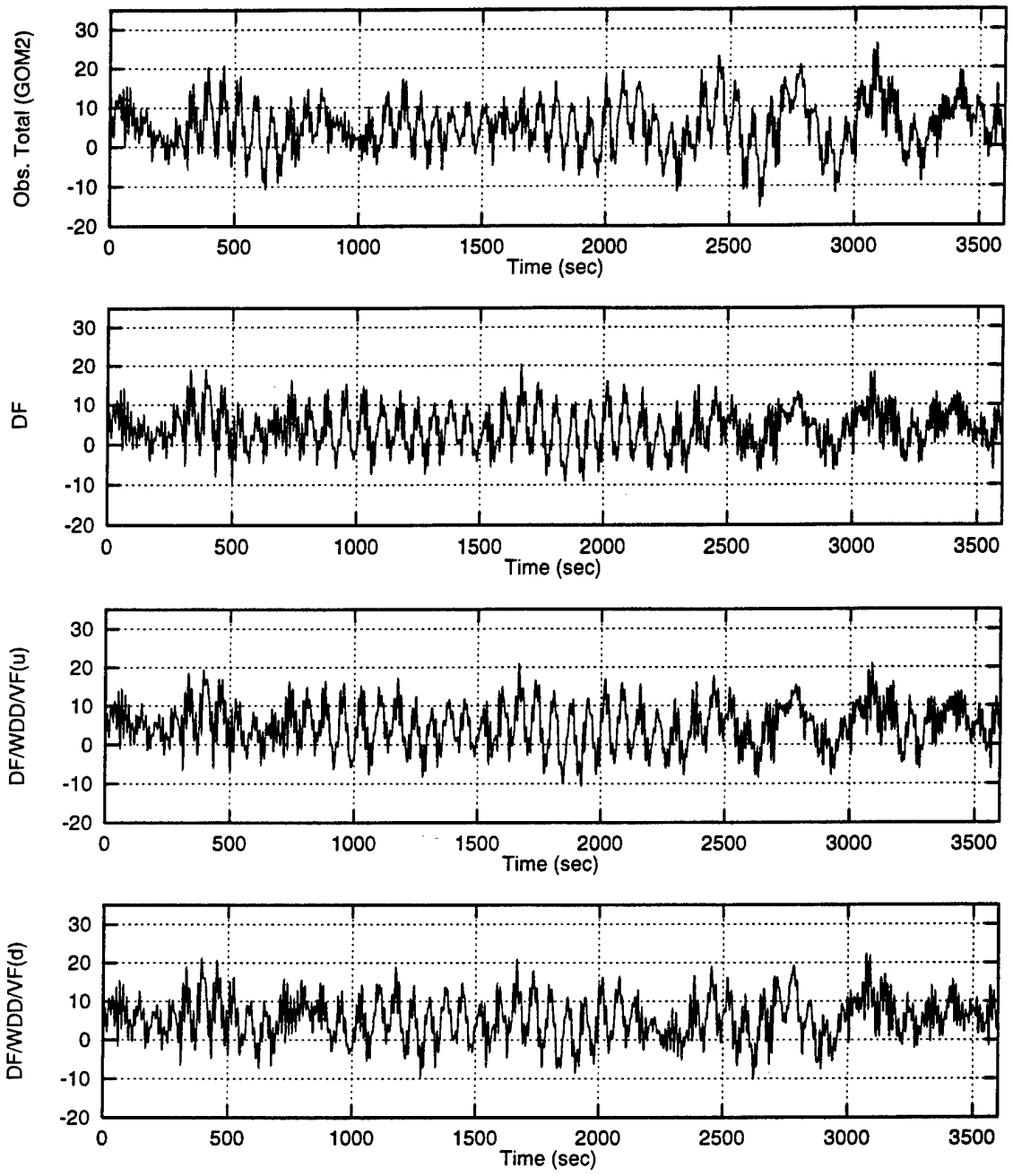

Figure 8: Combined (total) surge response time history for GOM2: prediction vs. measurement.

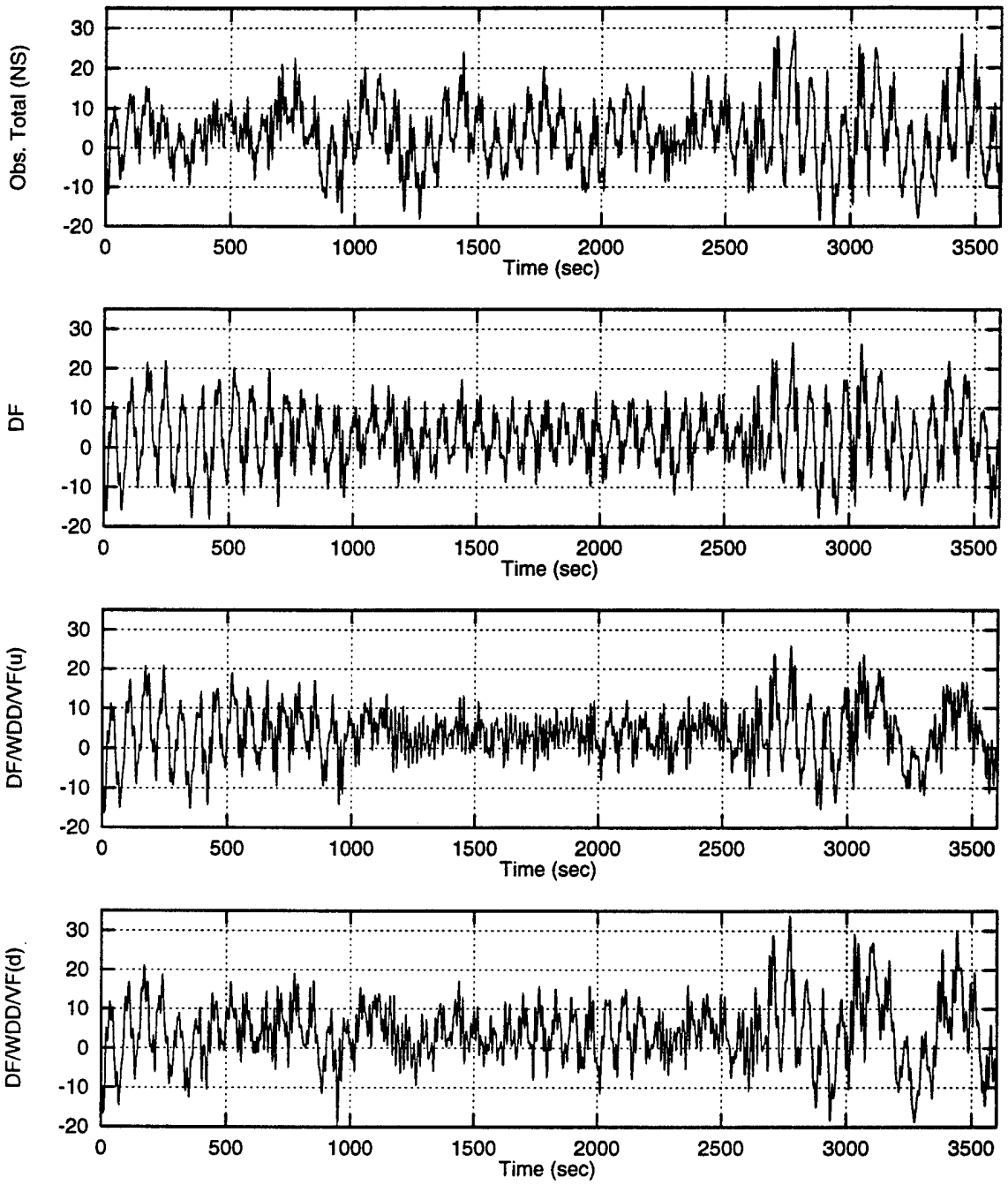

Figure 9: Combined (total) surge response time history for NS: prediction vs. measurement.

REFERENCES

Benjamin, J.R., Cornell, A.C., "Probability, Statistics and Decision for Civil Engineers", McGraw-Hill, 1970

Efron, B., Tibshirani, R.J., "An Introduction to the Bootstrap Method" Chapman & Hall 1993

Engebretsen, K., Winterstein, S.R.,"Probabilistic Specification of Metocean Criteria: Generating and Searching N-year Contours for Extreme Response Estimation", Relaibility of Marine Structures, TMS-32, Stanford, 1998

Faltinsen, O.M., "Sea Loads on Shi[s and Offshore Structures", Cambridge University Press, 1990

Fisher, R.A., "Moments and Product Moments of Sampling Distributions", Proceedings of the London Mathematical Society, Vol. 30, pp 199-238, 1928

Glanville, R.S, Pauling, J.R., Halkyard, J.E., Lehtinen, T.J., "Analysis of the Spar Floating Drilling Production and Storage Structure" Offshore Technology Conference, Houston, 1991

Johnson, N.L., Kotz, S., "Continuous Univariate Distributions-1", John Wiley & Sons, 1970

Jha, A.K., "QTF Surface Spline Interpolation: A Preprocessor to TFPOP", Technical Report, Reliability of Marine Structures, Stanford, 1996 (In TFPOP report RMS-18)

Jha, A.K., de Jong, P.R., Winterstein, S.R., "Motions of a Spar Buoy in Random Seas: Comparing Predictions and Model Test Results", BOSS, 1997.

de Jong, P.R., Winterstein, S.R., "Probabilistic Models of Dynamic Response and Bootstrap-Based Estimates of Extremes: The Routine Maxfits" RMS-34, 1998

Kahef, T., Winterstein, S.R., "Moment-based Probability Modeling and Extreme Response Estimation, the FITS Routine", RMS-31, Stanford, 1998

Kim, M.H., Yue, D.K.P, "The Complete Second-Order Diffraction Solution for an Axisymmetric Body. Part 1: Monochromatic Incident Waves", Journal of Fluid Mechanics, 200:235-264, 1998

Kim, M.H., Yue, D.K.P, Sum- and Difference-Frequency Wave Loads on a Body in Uni-Directional Gaussian Seas", Journal of Ship Research, 35(2):127-140, 1991

Madsen, H.O., Krenk, S.O., ad Lind, N.C., "Methods of Structural of Safety", Prentice Hal Inc., New Jersey (1986)

Massachusetts Institute of Technology, Department of Ocean Engineering, Cambridge. SWIM: Users manual.

Mekha, B.B., Johnson, C.P., and Roesset, J.M., "Non-linear Response of Spar in Deep Water: Different Hydrodynamic and Structural Models" 5th Offshore and Polar Engineering Conference, The Hague, The Netherlands, 1995

Melchers, R.E., "Structural Reliability; Analysis and Prediction", Ellis Horwood Ltd. 1987

Naess A., Røyset Ø., "The SRSS Formula for Prediction of Extremes of Linear Combination of Load Effects", OMAE98-1392, 1998

Newman, J.N., "Second-order, slowly varying forces on vessels in irregular waves", Proceedings International Symposium on Dynamics of Marine Vehicles and Structures in waves, p 182-186, Mechanical Engineering Publications 1974.

Ran, Z., Kim, M.H., Niedzwecki, J.M., and Johnson, R.P., "Responses of a Spar Platform in Random Waves and Currents (Experiment vs. Theory)", International Journal of Offshore and Polar Engineering, Vol. 6, No 1, March 1996

Rice, S.O., "Mathematical Analysis of Random Noise", Bell System Tech. Journal., Vol. 23 144, 282-332, 1944, and Vol. 24, 1945

Ude, T.C., "Statistics by Simulation from Second-Order Models of Response for Floating Structures", Proc. 10th ASCE Engineering Mechanics Specialty Conference, ASCE.

Ude, T.C., Kumar, S., Winterstein, S.R., "TFPOP 2.1: Stochastic Reponse Analysis of Floating Structures under Wind, Current, and Second-Order Wave Loads", Reliability of Marine Structures Program, Stanford University, RMS-18, 1996

Weggel, D.C., Roesset, J.M., Second-order Dynamic Response of a Large Spar Platform: Numerical Predictions Versus Experimental Results", OMAE 1996, Vol. 1

Wheeler, J.D., "Method for Calculating Forces Produced by Irregular Waves", Journal of Petroleum Technology, p 259-367, March 1970

Winterstein, S.R. and Ness, O.B., "Hermite moment analysis of Nonlinear Random Vibration", Computational Mechanics of Probabilistisc and Reliability Analysis, Elmepress 1989

Winterstein, S.R., "The FITS Routine: Fitting Distributions to Multiple Databases and Estimating combined Extremes", RMS-19, 1996

Winterstein, R.R., "Non-linear Vibration Models for Extremes and Fatigue", Journeal of Engineering Mechanics, ASCE, 144(10), 1772-1790, 1988

Winterstein S.R, Lange, C.H., "Moment-Based Probability Models for Wind Engineering Applications", Proceedings 10th ASCE Eng. Mech. Specialty Conference, Boulder Colorado, Vol. 1 1995, pp 159-163

Winterstein, S.R., Haver, S., "Statistical Uncertainties in Wave Heights and Combined Loads on Offshore Structures", Transactions of ASME, Vol. 113, pp 156-166, May 1991

REPORT DOCUMENTATION PAGE

Form Approved
OMB No. 0704-0188

1. REPORT DATE (DD-MM-YYYY)	2. REPORT DATE	3. DATES COVERED (From - To)
00-06-1999	June, 1999	

4. TITLE AND SUBTITLE

PREDICTION OF EXTREME RESPONSES FROM LIMITED DATA

5a. CONTRACT NUMBER

5b. GRANT NUMBER

N00014-96-1-0641

5c. PROGRAM ELEMENT NUMBER

6. AUTHOR(S)

P. R. de JONG

5d. PROJECT NUMBER

5e. TASK NUMBER

5f. WORK UNIT NUMBER

7. PERFORMING ORGANIZATION NAME(S) AND ADDRESS(ES)

RMS GROUP
S. R. WINTERSTEN, C. A. CORNELL
BLUME CENTER
STANFORD UNIVERSITY, CA 94305

8. PERFORMING ORGANIZATION REPORT NUMBER

RMS-36

9. SPONSORING/MONITORING AGENCY NAME(S) AND ADDRESS(ES)

OFFICE OF NAVAL RESEARCH
800 N. QUINCY ST.
ARLINGTON, VA 22217-4620
ATTN: DR ROSHDY BARSOUM

10. SPONSOR/MONITOR'S ACRONYM(S)

11. SPONSORING/MONITORING AGENCY REPORT NUMBER

12. DISTRIBUTION AVAILABILITY STATEMENT

APPROVED FOR PUBLIC RELEASE

13. SUPPLEMENTARY NOTES

14. ABSTRACT

This report documents a detailed study of procedures to estimate extreme responses to random excitation. Various methods are applied to predict the extreme statistics of the horizontal offset of a spar buoy, consisting of 3 dominant effects: Resonnant surge Resonnant Pitch, and wave-frequency effects. Both one hour of data and 36 hours of simulations are analysed. Gumbel, standard Weibull, quadratic Weibull are fitted using method of moments. Results of various methods are quantitatively compared.

15. SUBJECT TERMS

16. SECURITY CLASSIFICATION OF:			17. LIMITATION OF ABSTRACT	18. NUMBER OF PAGES	19a. NAME OF RESPONSIBLE PERSON
a. REPORT	b. ABSTRACT	c. THIS PAGE			19b. TELEPONE NUMBER (Include area code)